Master Thesis

submitted within the UNIGIS MSc programme
Department of Geoinformatics - Z_GIS
University of Salzburg

Land Cover Change and Landslide Susceptibility in Bogotá:

A case study in the eastern districts of the Colombian capital

by

Pia Teresa Kugel
105486

A thesis submitted in partial fulfilment of the requirements of
the degree of
Master of Science (Geographical Information Science & Systems) – MSc (GISc)

Advisor:

Dr. Daniel Hölbling

Ravensburg, March 5th, 2023

Acknowledgements

First of all, I would like to thank Dr. Daniel Hölbling for the supervision of this thesis, the continuous support and constructive feedback with specialised knowledge in the context of landslide hazards to advance this research and bring it to a successful conclusion.

Furthermore, I would like to thank the UNIGIS team for the great support throughout the Master´s study period.

A special thanks to IDIGER, the governmental institute in Bogotá for Risk Management and Climate Change, for providing all the landslide data used in this study.

I dedicate this work to my parents, who have always encouraged me throughout my studies and who unfortunately could not live to see the end of my studies.

Finally, I would like to express my sincere thanks to my husband Markus and children Paul, Miriam and Sofia for their patience and forbearance during the process of this thesis and the whole UNIGIS Master, especially in some difficult moments.

Inhaltsverzeichnis

INDEX OF FIGURES

INDEX OF FIGURES

INDEX OF TABLES

ACRONYMS

CBD	Central Business District
DANE	Departamento Administrativo Nacional de Estadística
ENSO	El Niño-Southern Oscillation
FR	Frequency Ratio
IDEAM	Instituto de Hidrología, Meteorología y Estudios Ambientales
IDECA	Infraestructura de Datos Espaciales para el Distrito Capital
IDIGER	Instituto Distrital de Gestión de Riesgos y Cambio Climático
ITC	Intertropical Convergence Zone
ha	hectare
LSI	Landslide Susceptibility Index
LSM	Landslide Susceptibility Map
NIR	Near-Infrared
NDVI	Normalized difference vegetation index
OBIA	Object-based image analysis
ONI	Oceanic Niño Index
POT	Plan de Ordenamiento Territorial
SDP	Secretaría Distrital de Planeación
SGC	Servicio Geológico Colombiano
SIMMA	Sistema de Información de Movimientos en Masa
SWIR	Short-wave Infrared
TIR	Thermal Infrared
TWI	Topographic Wetness Index
USGS	U.S. Geological Survey

Abstract

Bogotá, the capital of Colombia, is located on an altiplano in the eastern range of the Andean mountains at an altitude of about 2,500 m, in a topographically complex context, owned to the surrounding mountains with steep slopes to the east and south of the city. This research aims to analyse the landslide susceptibility in the eastern districts of Bogotá, namely Usaquén, Chapinero, Santa Fe and La Candelaria, based on a landslide inventory by IDIGER, which includes 464 landslides that occurred between 1996 and 2013.

To investigate the influence of land cover changes on the occurrence of mass movements, a multi-temporal land cover change assessment was carried out for the years 1985, 1997, 2014 and 2022. It can be concluded that an intensive process of settlement densification has taken place, and that the urban cover of the study area is expanding to the north and east, even in topographically unfavourable areas. An opposite trend can be seen in the increase of forest cover in the study area, which has a positive effect on the formation of landslides.

In addition to the land cover situation, nine other conditioning factors were identified and prepared for the Likelihood Frequency Ratio (FR) approach by classification. These ten parameters fall into three main categories: These are terrain derivatives (Digital Elevation Model, slope, slope aspect, curvature (plan and profile) and Topographic Wetness Index (TWI)), the category of landscape aspects (distance to watercourses and land cover) and finally geological aspects (distance to geological faults and geological categories).

The frequency ratio method relates the landslide ratio to the class ratio, i.e. the density of landslides per class to the percentage of that class in the whole study area. Each conditioning factor has a different frequency ratio, depending on the specific correlation between the class and the occurrence of landslides.

As a result, the Landslide Susceptibility Index for each point in the study area is presented on a map, divided into five categories of susceptibility: very high, high, moderate, low and very low. The result shows that the areas most prone to landslides are located at the foot of the mountain range. The influence of each parameter on the formation of landslides is then discussed.

In addition to geo-environmental factors, heavy rainfall plays an important role in the occurrence of landslides. For this reason, the phenomenon of La Nina, with its considerable influence on precipitation in the Colombian Andes, is discussed.

1. Introduction

2022 was the third consecutive year of the La Niña phenomenon, which affects many equatorial countries around the world. Colombia and its neighbours in the northwest part of South America are particularly affected by high rainfall and colder temperatures. As a result, in November 2022, Colombia declared a state of national disaster due to La Niña, stating that the heavy rainfall will increase the risk of subsequent flooding, flash floods and landslides. To support the emergency response to the ongoing disaster exacerbated by La Niña, the Colombian government received a US $300 million disbursement from the World Bank in December 2022 (WorldBank, 2022) .

To measure the power of natural catastrophes in Colombia there are some outstanding and devastating disasters, such as the eruptions of the *Nevado del Ruiz* volcano in November 1985, which caused a mud flow that killed more than 22.000 people, or the earthquake in Popayán in 1983, which also caused hundreds of deaths and massive destruction of infrastructure. However, in terms of frequency of natural disasters, landslides are a much greater hazard in the mountainous and hydrographically complex areas of the Colombian Andes. Occurring every year during the rainy months of spring and autumn, the exposure of settlements, infrastructure and people to this hazard should not be underestimated.

Bogotá Distrito Capital (D.C.), the rapidly growing capital of Colombia, is located in an intra-mountain basin called *Sabana de Bogotá* in the eastern mountain range of the Andes at an altitude of approximately 2.500m above sea level (Anselm et al., 2018). The *Páramo* and *Bosque Altoandino* ecosystems cover the surrounding mountains and represent a biodiversity hotspot in the tropical Andes. Their capacity to store large amounts of water supports the high freshwater supply of the megacity of Bogotá (Anselm et al., 2018). The pressure of migration to the city and the lack of habitable land in the Sabana, are spreading urbanisation to peri-urban areas, threatening this way the nearby ecosystems (Anselm et al., 2018). Unmeasured and unplanned urbanisation causes multiple negative impacts on society and economy, such as sealing of fertile soil, deaths related to pollution and heat waves or increased exposure to natural risks (Criado et al., 2020). The process of urban growth therefore plays an important role in the dynamics of land cover and land cover change (Rodríguez et al., 2013, Criado et al., 2020, Sánchez Cuervo et al., 2012, Romero et al., 2020).

Improving the knowledge of land cover and the dynamics in land cover change is essential given the continued expansion of megacities around the world (Romero et al., 2020). This becomes even more important in the face of the challenges of climate change, which has a strong impact on the living conditions of urban populations. Identifying hotspots of land cover change can help to design and implement policies to conserve the high and fragile biodiversity in the Andean region thus also protecting the people living in these fragile habitats (Sánchez Cuervo et al., 2012, Rodríguez et al., 2013).

In this research the hazard of landslide is analysed in detail to make evident where and why landslides occur and to relate this to the general susceptibility to this hazard in a particular part of the city, namely in the north-eastern districts. Susceptibility mapping is a popular method of visualising the zones that

are more prone to a particular natural hazard. There are many studies that focus on landslide susceptibility, mainly from countries that are highly exposed to landslide occurrence, such as China, Turkey, Austria (Görüm and Fidan, 2021, Abad et al., 2022, Goyes-Peñafiel and Hernandez-Rojas, 2021, Akgun et al., 2008, Zamora, 2018) applying different methods to calculate susceptibility.

In the literature can be found many papers which focus on the landslide risk and their impacts in the Colombian Andes (Aristizábal and Sánchez, 2020, Gómez et al., 2021, Sarmiento et al., 2015, Ramos et al., 2015b, Ramos et al., 2015a, Goyes-Peñafiel and Hernandez-Rojas, 2021, Zamora, 2018), some of them focus on the influence of precipitation (Ramos et al., 2015a, Aristizábal and Sánchez, 2020) and some few papers deal with landslide susceptibility mapping based on statistic Logistic Regression specifying the correlation between the different topographic factors and the risk of landslides (Goyes-Peñafiel and Hernandez-Rojas, 2021, Aristizábal et al., 2019, Zamora, 2018).

This thesis will carry out a multi-temporal assessment of land cover changes at different points in time to examine the impact on the frequency of landslides in the study area over the time. Trends in land cover change will be identified and related to the overall susceptibility. In a second step, other parameters that influence the occurrence of landslides to varying degrees will be identified and analysed. The final objective is to produce a map of landslide susceptibility using the Likelihood Frequency Ratio model, taking into account land cover and nine other relevant factors to create a reliable and useful visualisation.

2. Study area and Data

2.1. Study area

The study area in this research are the north-eastern *localidades* of Bogotá*,* from now on called districts. The four districts of interest, namely Usaquén, Chapinero, Santa Fe and the smallest one, La Candelaria, form the boundary with the oriental mountain range that starts just in the east of the city. The study area extends over 30km from north to south and about 9km at its biggest extent from west to east and comprises a total area of approximately 152,5 km^2 with 882.000 people living there as at 2022 (SDP, 2022). It is located at 4°41’’’N and 74°2’37’’W.

The district of Usaquén has the biggest extension with about 65 km^2, Chapinero extends over 39 km^2 and Santa Fe 45 over km^2. La Candelaria, lying fully within Santa Fe, has only a size of 2,1 km^2 and is with this the smallest district in the city. However, La Candelaria is the historic and cultural heart of the city, being there the *Plaza de Bolívar*, Colombia´s biggest place, several universities and the Cathedral of Bogotá (Abad et al., 2022, Aristizábal and Sánchez, 2020). These four districts form the historic centre, characterized by the Spanish colonial style, visible in the architecture and in the rectangular ground-plan of the streets. Besides being the historic centre, Chapinero is also the financial and commercial heart of Bogotá. Several banks and commercial centres are located here in the Central Business District (CBD) making it to a wealthy and prosperous district. With the exception of La Candelaria, the municipal boundaries of Usaquén, Chapinero and Santa Fe extend well beyond the actual urban area, including parts of the mountainous hinterland, as shown in figure 4.

Figure 1: Colombia in the World

Figure 2: The country Colombia

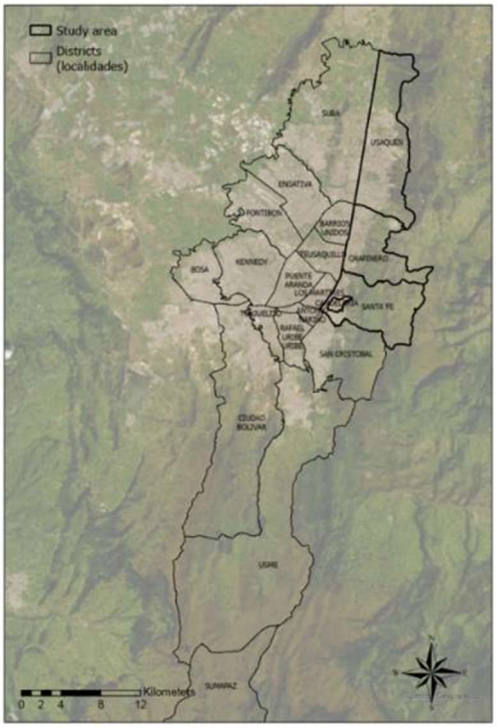

Figure 3: The 20 districts of Bogotá D.C.

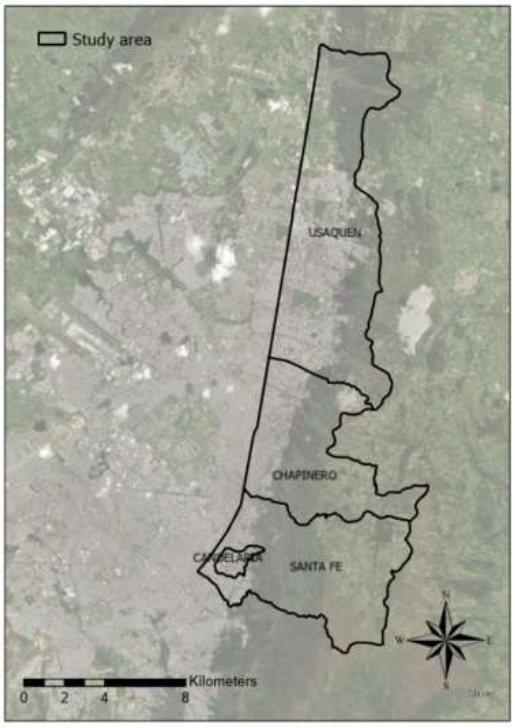

Figure 4: Study area in Bogotá D.C.

2.1.1. Topography

The country Colombia is located in the tropes, divided by the equator in the south of the country.

The mountain range of the Andes passes through the country from the South to the North and splits up in three *cordilleras*, the Western, the Central and the Eastern Cordillera. Colombia borders on two Oceans, the Caribbean Sea and the Pacific Ocean. The country disposes over any type topography, from high mountainous areas to swamp and thickly wooded jungle. Based on this topography, the country can be divided into five very distinct natural regions (Aristizábal and Sánchez, 2020): The Caribbean, the Orinoco and Amazonas regions are very flat, while the Andean region is characterized by high mountainous environment. As a consequence of these topographically very different regions, the natural hazards the country faces are very diverse. Located on the eastern section of the *Pacific Ring of Fire*, where much of the world´s earthquake and volcanic activity is concentrated, makes the country very susceptible to these hazards.

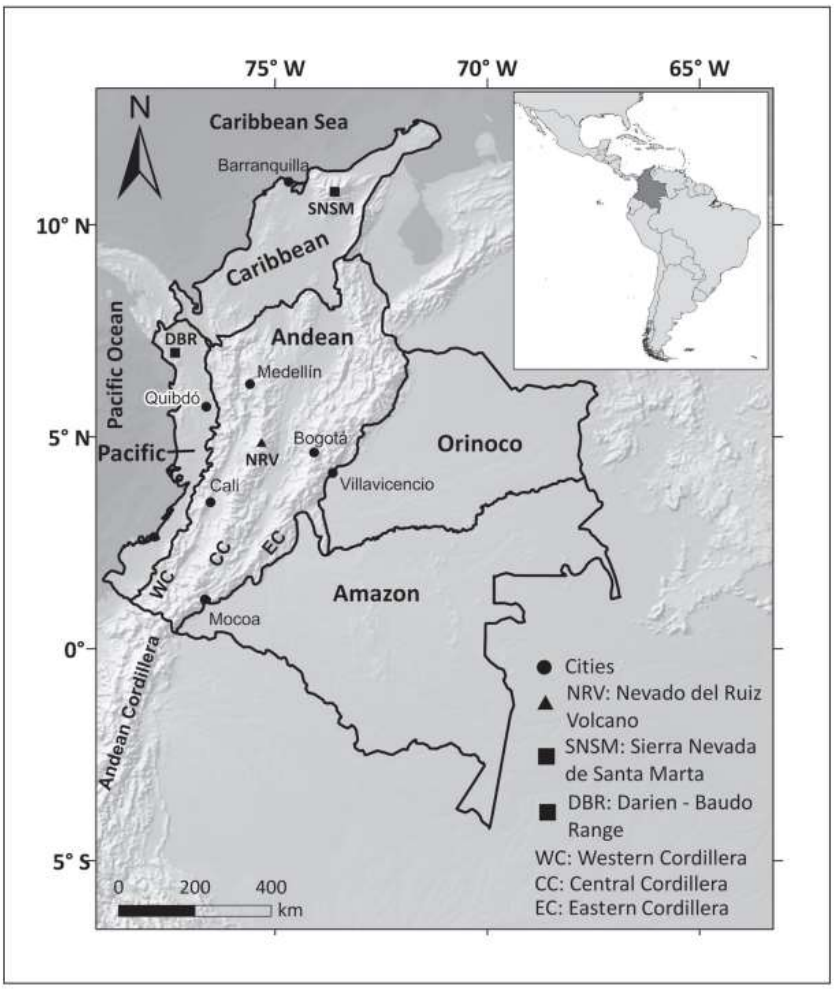

Figure 5: Locations of and regions in the Colombian Andes (Aristizábal and Sánchez, 2020)

Bogotá itself is located in the *Sabana de Bogotá* and extends from 2500 to 3700m on the Eastern cordillera. The city can be roughly divided into two parts: the flat areas in the western and northern parts of the city, and the mountainous areas in the eastern and southern parts.

2.1.1.1. Digital Elevation Modell

The Digital Elevation Modell (DEM) is an indispensable tool to visualize the topographic situation in a certain area. This 3D-view shows the enormous differences in altitude of more than 1.000m within a small geographic area. The flat area of the Sabana appears in green and shows nearly no slopes. Nevertheless, the yellow stripe indicates already altitudes of up to 3.000m, belonging still to the populated area. The highest elevation can be seen in the south, in Santa Fe, while the altitude of the mountains decreases towards the north.

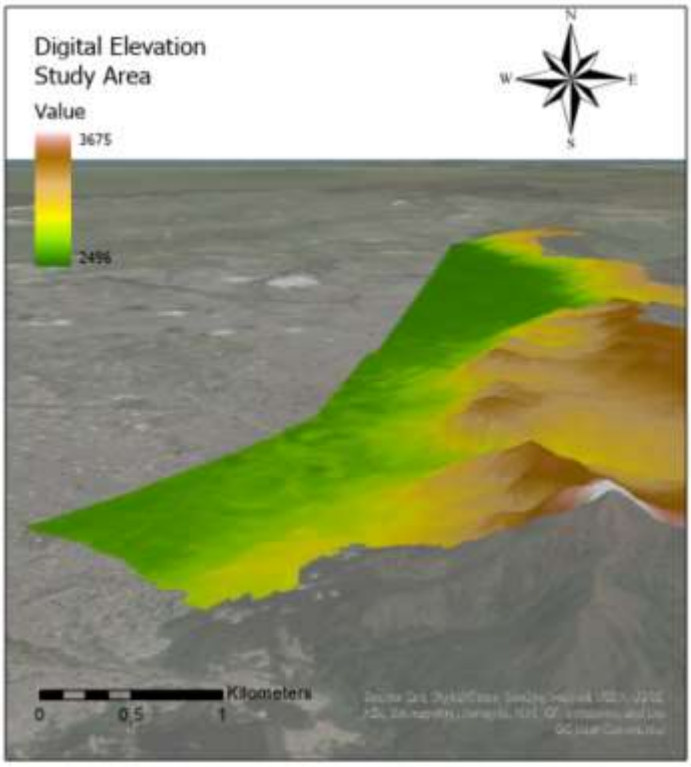

Figure 6: 3D View on the Study area (USGS_Earth_Explorer, 2013)

2.1.1.2. Geology

The Sabana de Bogotá arose in the Quaternary, in the time episode called Pleistocene which is relatively young. This Sabana, was a big lake in the era of Pleistocene, that began before 2.6 million years and ended about 12.000 years ago. During this period, average temperatures were much lower than they are today, and huge glaciers formed in the mountains. The valleys of the rivers that cross the altiplano still contain evidence of this period. The basin is filled with Pliocene to Quaternary fluvial lacustrine deposits (Anselm et al., 2018). The ground of this former lake is soft but since it is mainly clay, up to 10 meters deep, with sand, gravel and organic layers further down, it is also thick and seismic waves can be amplified dramatically and travel through long distances. These characteristics of the ground do at the same time not allow the water to seep away quickly (Yamin. L. E.; Ghesquiere, 2013).

The oriental hills are mainly composed out of sandstone (Ksglt) and clay and siltstone (Ksgp). These types of soil work as a sponge and can gather high sums of rainwater, but, on the other hand if they have absorbed to much water, this kind of ground will also promote landslides.

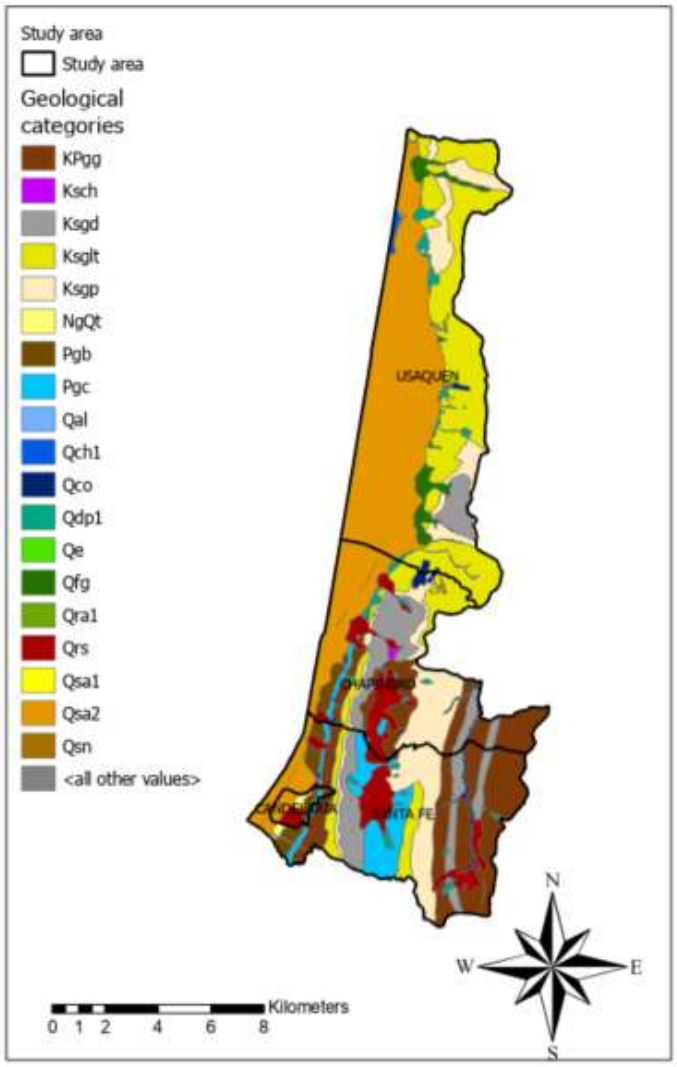

Figure 7: Geological categories in the urban zones of the Study area (IDECA, 2022c)

Table 1 shows the different geological classes appearing in the study area, grouped into five major categories that will later be used to prepare the susceptibility maps. There are several classes called formations, which seem to be very specific to this geological zone in Colombia.

Category	Abbreviation	Name	characteristics
Alluvium	Qal		Alluvial deposit
	Qch1	Chia Formation	flood clay, organic clays
	Qco		Colluvial deposits, embedded in clay
Clay	KPgg	Guaduas Formation	Clay with quarzarenite
	Ksgp	Plaeners formation	clay, siltstone
	Pgb	Bogotá Formation	clay, sandstone
	Qsa2	Sabana Formation	clays
	Qsn	black floors	clays
	Qrs	Siecha River Formation	blocks of fluvio-glacial origin with sand and clay
Deposits	Qdp1		Slope deposit
	Qe		Anthropic debris deposit
	Qfg		Fluvioglacial Reservoir
	Qra1		Anthropic fillers
Limestone	Ksch	Chipaque Formation	limestone, shale
Sandstone	Ksgd		sandstone formation
	Ksglt		Sandstone
	NgQt	Tilatá formation	sandstone
	Pgc	Cacho formation	sandstone
	Qsa1	Sabana Formation	shales, sandstones

Table 1: Overview of all geological categories (IDECA, 2022b), own figure

2.1.1.3. Fluvial Network

In the context of landslides, the fluvial network is important to understand. The main basin to which all rivers, streams and canals belong is the Bogotá River Basin. The Bogotá River drains the whole area and is tributary of the Rio Magdalena, a 1.600km long river in the western part of Colombia, passing from the south to the north flowing into the Caribbean Sea.

The origin of the Bogotá River is in the north of the city and it passes the city from the north to the south through the western part of the Sabana. It has a length of only about 200km but it can be optimally used for generation of water energy due to enormous differences in altitude. In the city itself the river suffers from massive pollution due sewage and waste water from adjacent industries.

On the IDECA homepage can be found a database containing all rivers, basins and water bodies of the city of Bogotá (IDECA, 2021). Including the drainage system this database counts with 13.280 entries. Filtered for the study area there still remain 919 water courses, belonging all to the Bogotá River basin. This basin can be further divided into the subbasins of Río Fucha, Río Salitre, Río Teusacá and Río Torca and their respective numerous microbasins.

Figure 8 shows the distribution of water courses in the study area. The absolute majority represents the group of drainage canals. In the explanations of IDECA (IDECA, 2021) they are described as every basin o watercourse that does not belong to any other defined group, such as river, stream or canal. Nevertheless, they play an essential role in the hydrological context of the mountainous region of the Study area.

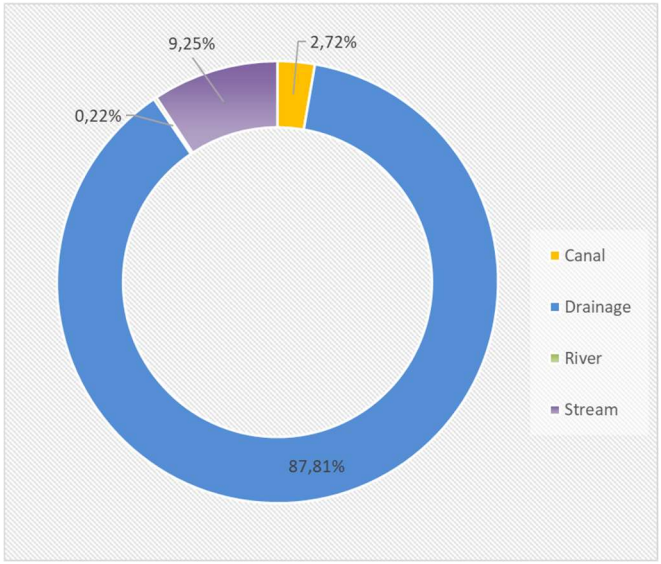

Figure 8: Percentage of water courses in the Study area (IDECA, 2021)

Figure 9 illustrates the affluents and drainage system of the four subbasins of the Bogotá River. All the drainage course, belonging to Río Torca, Río Salitre and parts of Río Fucha flow down the mountains until the beginnings of the settlements. The purple subbasin, the Río Teusacá drains to the eastern side.

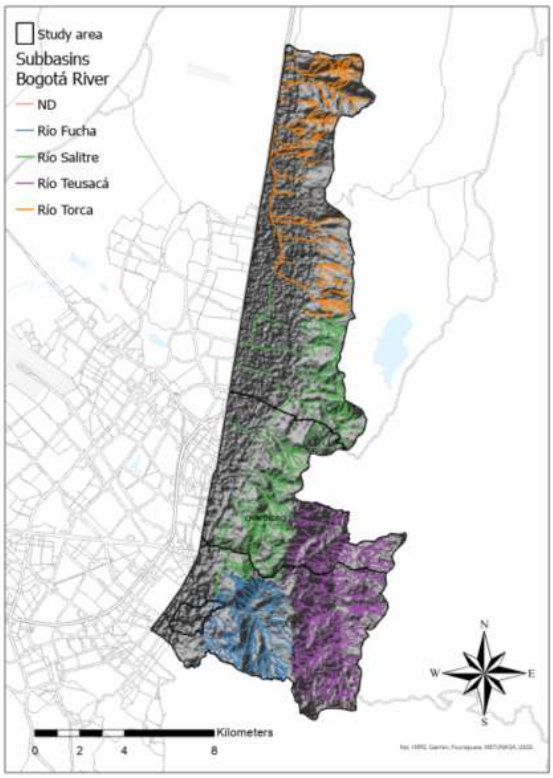

Figure 9: Affluents and drainage system, Bogotá River in the Study area (IDECA, 2021)

2.1.2. Climate

2.1.2.1. Temperature and precipitation

Despite its location in the tropes, at 4 degrees north latitude, just north of the equator, Colombia is a climatically diverse country due to its very varied topography. For a better understanding of Colombia´s climatic zones, the Köppen-Geiger climate classification has been chosen, which divides the world´s climates into five main groups: **A** (tropical), **B** (arid), **C** (temperate), **D** (continental) and **E** (polar) (Worldbank, 2021). All climates except those in group E, the polar group, have been assigned a second minuscule for the subgroup describing seasonal precipitation.

The Amazonas and Orinoco region in the east are characterized by a tropical climate, *Af* and *Am*, signifying that there is rainfall all over the year without distinctive rainy seasons. The Pacific region is also characterized by hot and wet climate zone *A*f and precipitation throughout the year while the Carribean cost belongs to *Aw* meaning that in the winter months there is less precipitation, i.e., a dry season.

Although located within the tropical zone, the Andes have green raster cells what indicates a temperate climatic zone due to their altitude. Following this rough structure, Bogotá would belong to

the climate zone *Cfb*, what means that the warmest month is below 22° and also rainfall throughout all months.

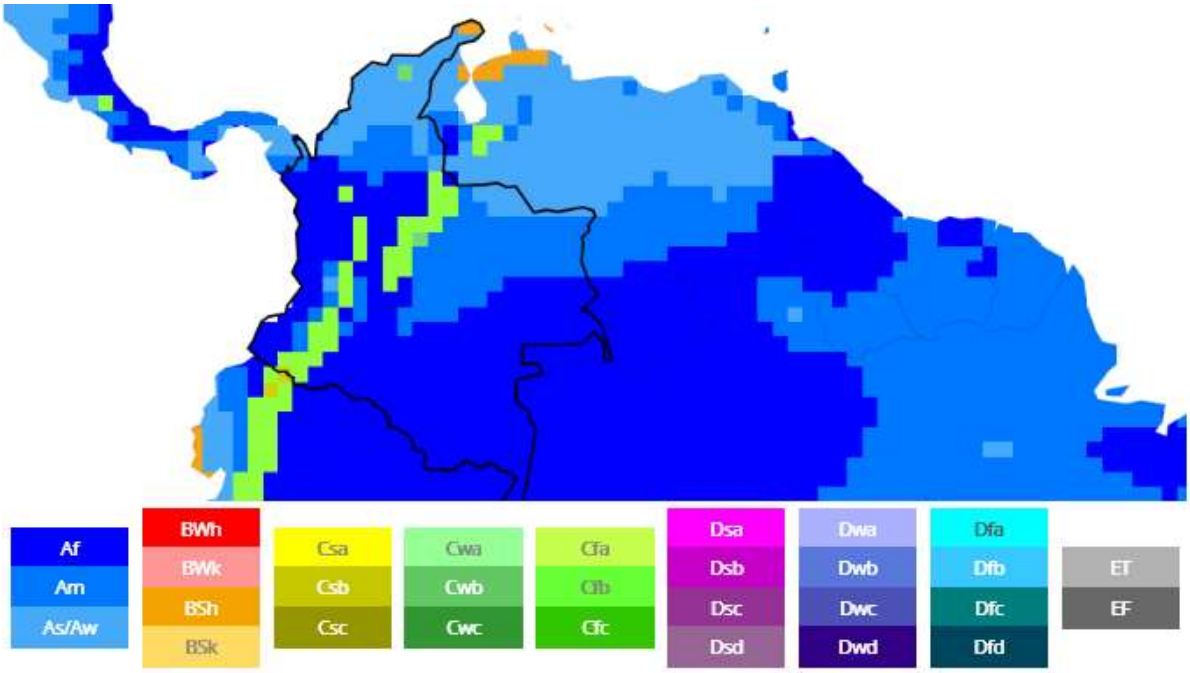

Figure 10: Köppen-Geiger Climate Classification 1991-2020 (Worldbank, 2021)

In Colombia, the annual hydrologic cycle is controlled by oscillation of the Intertropical Convergence Zone (ITC). It is superimposed on regional climatic characteristics caused by the orographic influence of the Andes, evapotranspiration in the Amazonas Basin and dynamics out of the western wind currents (Hoyos et al., 2013).

The temperature in Bogotá is constantly during the whole year with a slight minimum in the months of June, July and August. The average maximum temperature is about 17 degrees, which is significantly lower than in the plane areas of the country. According to the climate diagram of Diercke Global Atlas (DierckeAtlas, 2022) Bogotá has a mean annual temperature of 13,3°C and mean annual precipitation of 824mm.

The precipitation is not equally distributed around the year, but there are two maxima, in the months of April and May and the other one in October and November, this happens due to the location within the ITC. The eastern Andes are exposed to trade winds, which create humid and rainy conditions; the western Andean region, near the Pacific have even higher annual precipitations while the inter-Andean valleys are less humid (Rodríguez et al., 2013).

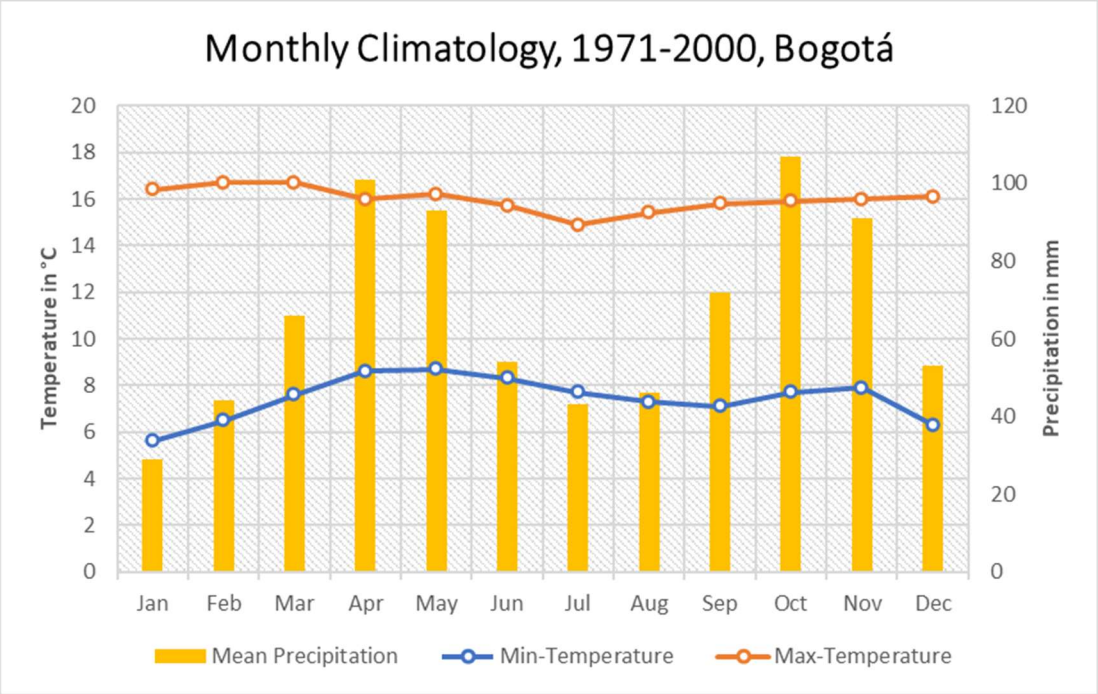

Figure 11: Monthly Climatology Bogotá, average values for 1971-2020 (WMO, 2022)

It is also interesting to see the great differences in amount and temporal distribution of rainfall within the city of Bogotá. In the southern part, above all in the top zones the peaks of precipitation are much higher than in the mean zones (Ramos et al., 2015a). In the eastern part, and on the foot of the mountains the sums are considerably higher. It can also be observed that the western slope aspects of the mountain ranges are greener, with denser vegetation than the eastern slopes indicating that precipitation must be higher on this side.

2.1.2.2. The La Niña phenomenon

The most known climatic phenomena with extensive consequences for the whole continent of South America, but especially to Colombia, is the so called El Niño and, the opposite pattern, the La Niña phenomenon.

For measuring and monitoring these phenomena the primary indicator in the Oceanic Niño Index (ONI) or El Niño Southern Oscillation (ENSO). The ONI tracks the running 3-month average sea surface temperatures in the east-central tropical pacific between 120°C – 170°C to monitor if they are warmer or cooler than average to draw conclusions if it is about a La Niña or El Niño phase or neutral conditions prevail. ONI values indicate the climate phenomenon, if they differ more than 0,5°C from average (NOAA, 2022). Negative values indicate the occurrence of La Niña phenomenon, positive values indicate El Niño.

The warm phase, i.e. El Niño, is associated with an increase of air temperature and a decrease in evapotranspiration and rainfall intensities and in the following a decrease in soil moisture and average flow of rivers (Hoyos et al., 2013). La Niña however, brings cooler-than-average waters to the central

and eastern tropical Pacific and the prevailing easterly winds intensify. Depending on its intensity, La Niña brings high volumes of precipitation to some regions of Colombia (Ramos et al., 2015a).

A correlation between the formation of La Niña years and streamflow records can be observed throughout Colombia (Poveda et al., 2001). However, ENSO events differ in intensity and spatial extent and subsequently also their effects on hydro-climatology (Hoyos et al., 2013). Nevertheless, the massive rainfalls have also an influence on the quantity of landslides in the mountains of Bogotá (Ramos et al., 2015b). To visualize the correlation between the occurrence months of landslides and the ONI in Bogotá the IDIGER 4 database has been overlaid with the ONI for the years 1996-2016. In the below graphic the La Niña episodes of 1998-2000, 2010-2012, 2017-2018 and La Niña episode started in 2020 are marked. The landslides out of IDIGER 4 with 3.885 landslides have been used to have the highest possible number of events to show a statistical correlation between the value of the ONI and the number of landslides.

Of course, it is not the ONI itself that triggers the landslides but the precipitation of the phenomenon the ONI indicates. There is always a 1-2 month lag between extensive rainfalls and the occurrence of devastating floodings and following landslides (Ramos et al., 2015a). Therefore, for the current La Niña phase there are still landslides to expect. The ONI values for the year 2022 are between -0,8 and -1,1 and show a persisting negative curve.

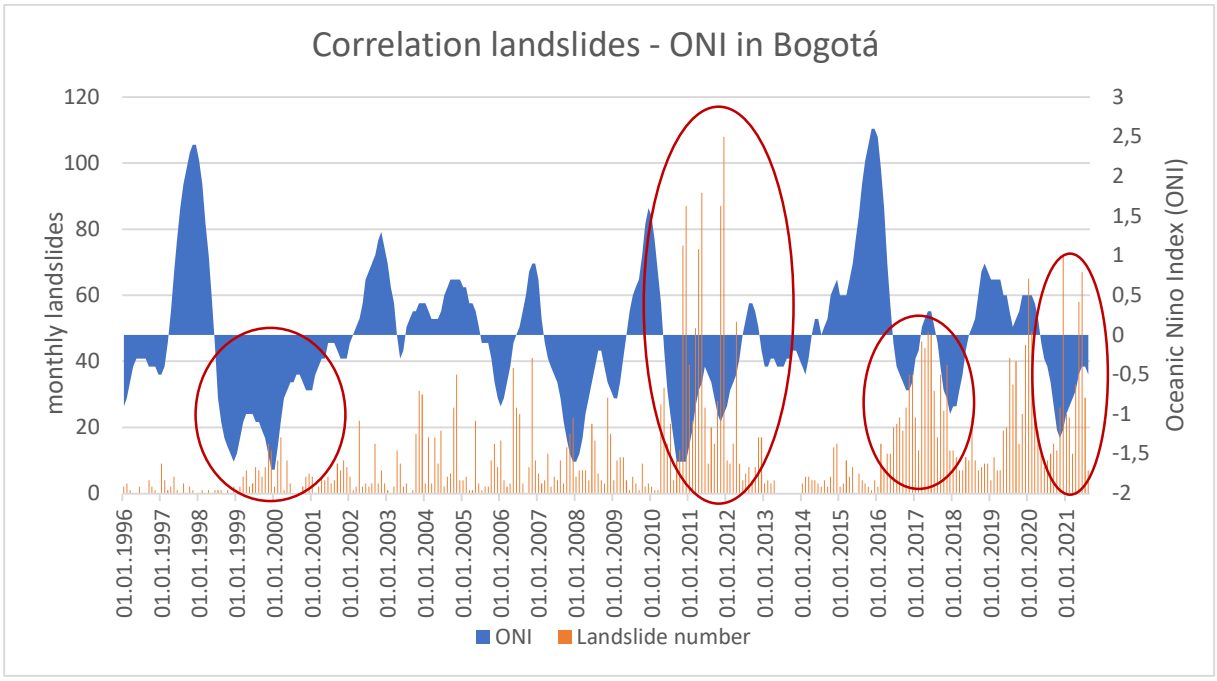

Figure 12: Correlation between number of landslides (IDIGER 4) and the Oceanic Niño Index (ONI) (ClimatePredictionCenter, 2022, Ramos et al., 2015a), own figure

2.1.3. Population

2.1.3.1. Development

In 2022 there are about 52m people living in Colombia, the second biggest country in South America. Bogotá is the biggest and economically most important city in Colombia. Regarding its size, Bogotá takes the 4th place in South America with 7.67m people living in Bogotá D.C. In the greater metropolitan area there are about 11,27 m people living (SDP, 2022, PopulationStat, 2022). The next two big cities, Cali and Medellín count with 2.4mn and roughly 2m people.

Bogotá accounts for more than 20% of the population of Colombia (Romero et al., 2020). Looking at the statistics, the enormous growth rate of up to 25%, seen in the 60s until the 80s of the last century is over and the dynamic has slowed down over the last decades and will even slow down more in the future. Nevertheless, the growth rate in 2025 will be still about 4% (on a higher level of inhabitants) and the number of inhabitants will in a consequence increase steadily up to more than 9m people in 2050 only in the city. The total urban area will count with up to 12m people in 2050 (PopulationStat, 2022). Bogotá is taken as one of the main developing megacities in Latin America (Romero et al., 2020).

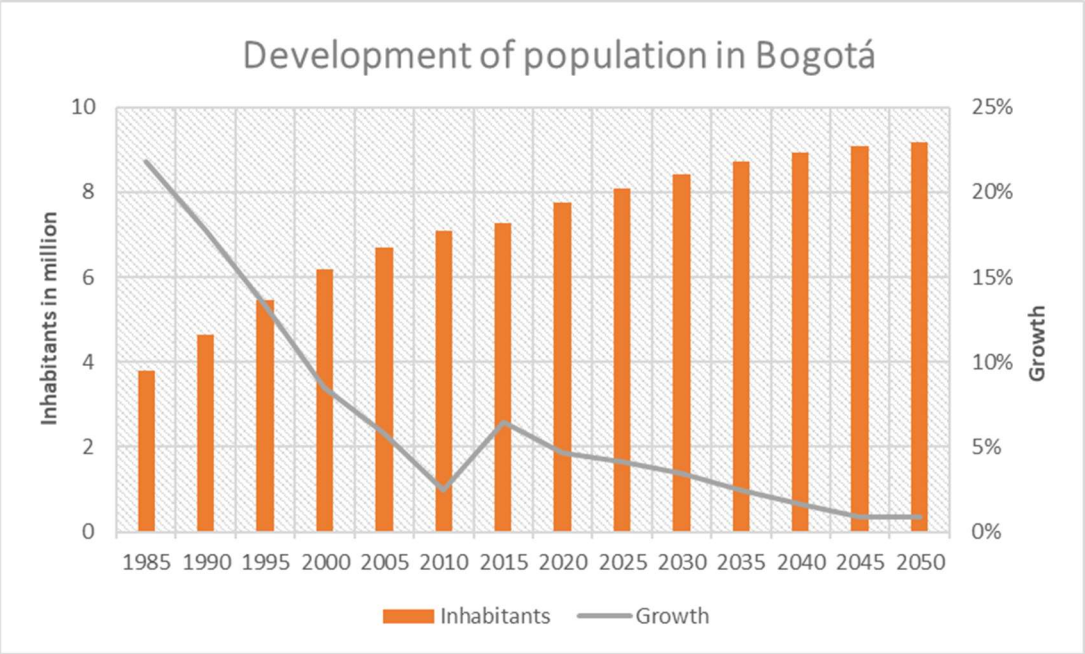

Figure 13: Development of population in Bogotá D.C. (SDP, 2022)

The expansion of the city had different drivers: first, a distinctive migration movement from rural to urban areas. Bogotá promised a wealthy and prosperous live attracting thousands of people per year, while the live in the rural areas was meagre and exhausting. Second, beside poverty in the rural regions, an important reason have been internal displacements caused by the social and armed conflicts during the 1990s and in the first decade of the 21st century (Romero et al., 2020) that led to the disproportional high growth rates.

Usually, the megacities in the world grow without proper planning, their growth is a consequence of demographic growth and migration towards them (Yamin. L. E.; Ghesquiere, 2013). Therefore, residential areas grow without control in the suburban areas even though the topography is not

favourable for construction of houses. In the case of Bogotá, residential areas can be found through the whole city, but the poorer settlements are on the outskirts of the city.

Nowadays, migration towards Bogotá continues, on the one hand internal migration, on the other hand, there can be identified a movement from migrants out of Venezuela and other countries in precarious conditions. Subsequently, number of inhabitants is still increasing and the question remains, where has the city still enough space to allow new settlements. As the inner city has no more capacities due to the dense buildings, the arriving people will look for a place in the suburban areas. The strong migration pressure in the past led to the fact that the slopes of the mountains have been deforested and partly build up with settlements and houses not considering the high vulnerability of these zones, out of ignorance or helplessness (Yamin. L. E.; Ghesquiere, 2013). As a consequence, the exposure to natural hazards such as landslides, has increased over the last decades, living now much more people in regions of high risk.

The situation in the study area presents itself as follows. Since 2005 there is a significant decrease in population growth, from more than 4% in Usaquén and Chapinero to now below 2%. The number of inhabitants in La Candelaria is growing but on a low level, while the growth rate in Santa Fe remains stable.

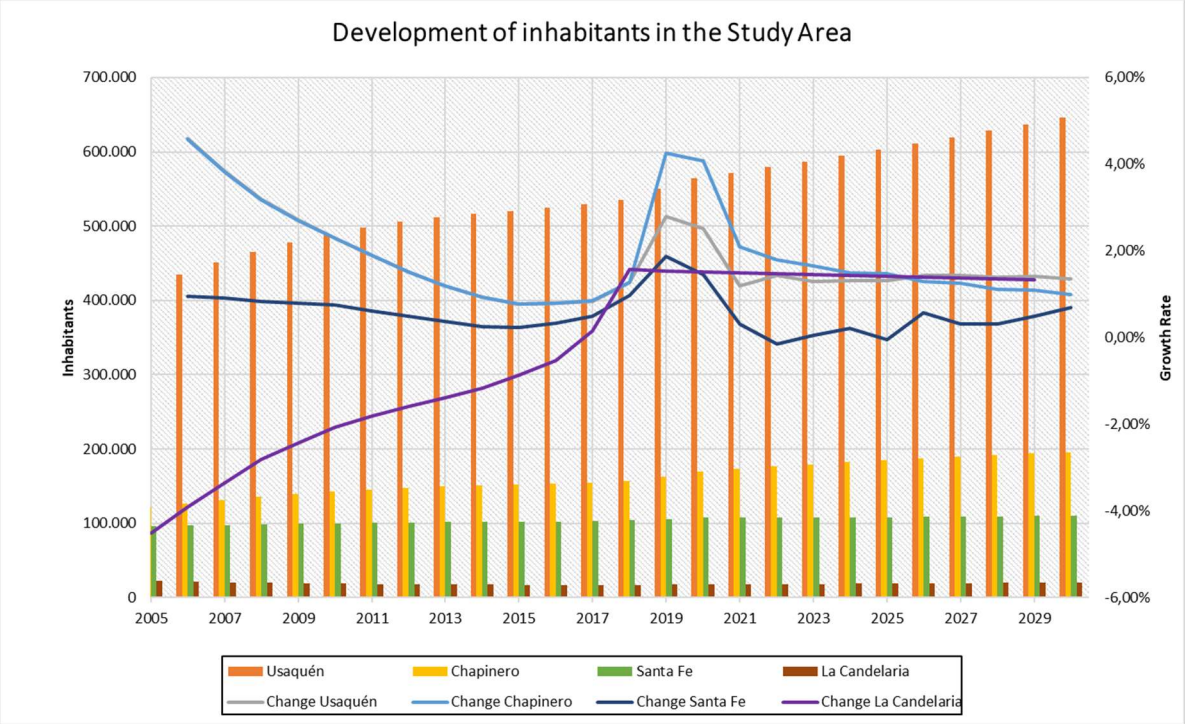

Figure 14: Number of inhabitants and growth of population in the study area (SDP, 2022)

Table 2 summarizes the demographic situation in the study area. Looking at the time period since 2005 the district Usaquén grew by almost 40% and Chapinero even by 45%, evolution which shows the high populational dynamic here. In 2022 in Usaquén and Chapinero were living more than 750.000 people

Parameters	Usaquén	Chapinero	Santa Fe	La Candelaria
Size	66,16 km^2	38,62 km^2	45,74 km^2	2,1 km^2
Inhabitants 2022	579.447	176.471	107.630	18.143
Population Growth 2005-2022	39,6%	45,5%	12,1%	-18,6%
Inhabitants per km^2	8.758 p/ km^2	4.569 p/ km^2	2.353 p/ km^2	8.639 p/ km^2
Rate of unemployment 2017	6,31%	4,05%	10,06%	8,54%

Table 2: Overview of the Study area (SDP, 2022, IDECA, 2022)

SDP, the source of this data, makes a difference in the calculation of inhabitants. As the districts include also parts of areas which are populated by only very few people there are two options to choose: *Localidad*, which means the whole area, and *Cabecera* which includes only the areas belonging directly to the city. I chose the inhabitant number for the whole district, knowing that the parameter inhabitants per hectare is rather low then, as the square kilometers of the total district are considered for calculation.

The distribution of inhabitants is not proportionally throughout the city, looking at the figure 15 from SDP. Kennedy, Bosa, San Cristóbal and Rafael Uribe Uribe have the highest rates of density with up to 310 inhabitants/ha. These districts can be found in the south and west of Bogotá.

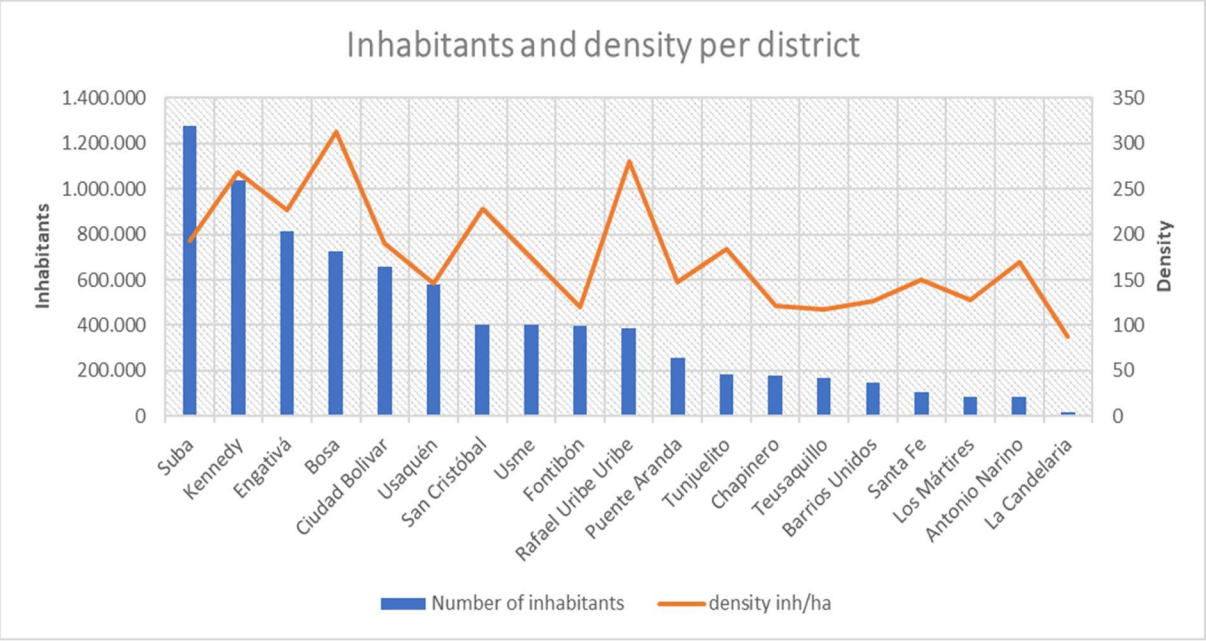

Figure 15: Inhabitants and density in the districts of Bogotá in 2022 (SDP, 2022)

Figure 16 shows the density of population (inhabitants/ha) in the whole city of Bogotá, with a higher resolution than on district level. The majority of people lives in the western and southern districts, coloured in red showing a density of up to 1.115 inh/ha. Usaquén has the highest number of inhabitants in the Study area, but all the four districts are coloured predominantly in green and yellow as density is in comparison to other zones of the city not that high.

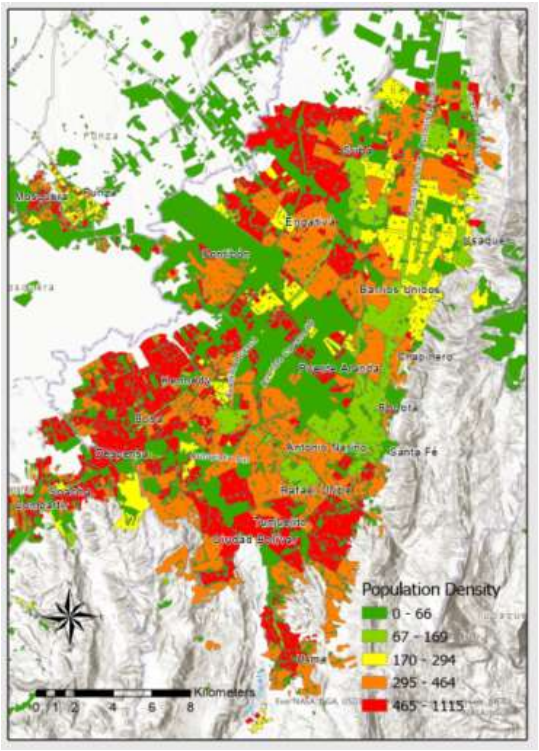

Figure 16: Density of inhabitants in Bogotá (Chavez, 2019)

2.1.3.2. Socioeconomic stratification

The density of inhabitants is a first indicator of the social stratification within a city. Due to the strong migration of people from rural regions in the last decades towards the megacity of Bogotá, people were seeking new land to live. Low-income inhabitants were pushed out to the city´s outskirts and promoted this way the growth and development of the city (Romero et al., 2020). Obviously, the topographic conditions were not favourable for settlements due to mainly mountainous conditions with poor infrastructure such as water, electricity and transport connections. The legalised settlements can be seen in figure 17. A high density of settlements can be noted in the south of the city, but also within the study area especially in Santa Fe and in the north of Usaquén.

Generally speaking, Chapinero and Usaquén are both inhabited by upper class neighbourhoods considered as some of the most attractive and popular areas in Bogotá, visible also in the relatively high growth rate of population. The majority of this districts extends over the mountain range and is only sparsely populated. Subsequently, the density of population is quite low. Santa Fe and La Candelaria differ in their social structure visible in the smaller, or even negative growth rate of population and their higher rate of unemployment (table 2). These districts were in parts no-go areas and had to deal with high criminality rates in the past.

According to the socioeconomic stratification, the city has a clear social structure. There are seven different strata, defined by the number of households which rely on public services (DatosAbiertosBogotá, 2023). The northern and north-eastern part of the megacity belong to the wealthy zones, coloured in blue and belonging to stratum 5 and 6. The study area is mainly located in this zone, but there can be found red zones in Santa Fe and in the north of Usaquén and along the mountains as well. Generally speaking, the further south, the more yellow and red zones appear indicating a lower socioeconomic stratum. This structure coincides with the map of population density. The higher the density the lower is the socioeconomic stratification.

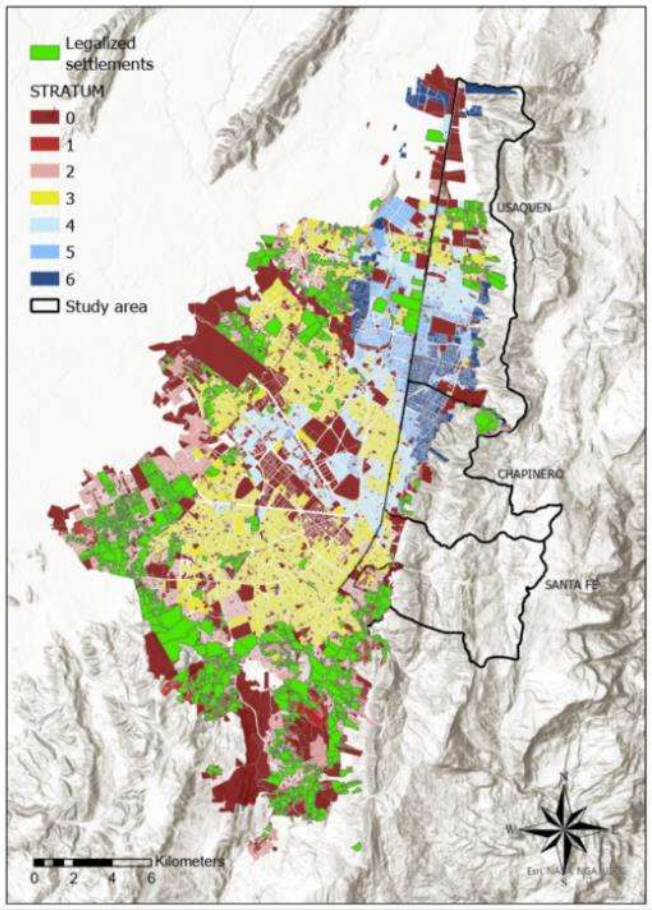

Figure 17: Stratification and legalised settlements in Bogotá (DatosAbiertosBogotá, 2023, IDECA, 2022a)

2.2. Data

This research uses ArcGIS Pro 3.0, an ESRI product, for the processing of landslide data, the creation of the land cover maps and the additional analytical maps with the aim of generating a susceptibility map for the Study area. ArcGIS Pro was chosen as it is a very powerful tool with many automated processes, especially for the image classification and comparison.

To begin the GIS-based temporal land cover assessment and landslide susceptibility analysis, data must be collected from different areas. The relevant data are shown in table 3.

A meaningful susceptibility map is obtained by overlaying various geo-environmental factor maps. These factors, which contribute to different extends to the landslide occurrence are combined with a landslide inventory based on historical landslides.

Name	Dataset	Source	Creation date	Type of data
Landslide inventory	Landslide inventory	IDIGER, combination of different datasets	2022	Point data
Satellite data	Landsat images	USGS Earth Explorer: Landsat 9 Image 2022: LC09_L2SP_008057_20220131_20220202_02_T1 Landsat 8 Image 2014: LC08_L2SP_008056_20140101_20200912_02_T1 Landsat 5 Image 1997: LT05_L2SP_008057_19970830_20200909_02_T1 Landsat 5 Image 1985: LT05_L2SP_008057_19850322_20200918_02_T1	2022	Tiff/ 30m resolution
Terrain derivatives	ASTER Digital Elevation Modell (DEM)	USGS Earth Explorer: ASTGTMV003_N04W074_dem/ ASTGTMV003_N04W075_dem (Acquisition date 2000-2013)	2022	Tiff/ 30m resolution
	Slope	Derived from ASTER DEM		Raster
	Slope Aspect	Derived from ASTER DEM		Raster
	Curvature Plan	Derived from ASTER DEM		Raster
	Curvature Profile	Derived from ASTER DEM		Raster
	Topographic Wetness Index	Derived from ASTER DEM		Raster
Landscape factors	Distance to drainage	IDECA	2022	Line data
	Landcover	Prepared with Landsat images	2023	Raster
Geological factors	Distance to faults	IDIGER	2022	Line data
	Geology	IDECA	2023	Polygon shapefile

Table 3: Data used for susceptibility mapping, own figure

The factors from this table are intended to contribute to the production of a susceptibility map. The climatic factors are not included in this list and do not play a role in the statistical approach. Nevertheless, the effect of the La Niña phenomenon will be included in the discussion below to highlight the correlation.

2.2.1. Hazards

2.2.1.1. Types of hazards in Colombia

Bogotá is exposed to many different kinds of natural hazards due to its exposed geographical, topological and hydrogeological place in the Andean mountains. The below chart serves for an overview of all hazards, not limited to natural hazards, occurred in the city of Bogotá. This graphic makes evident that the highest percentage in hazards is owed in the first place to floods, followed by fire and already on the third place can be found landslides. Desinventar (Desinventar, 2020) does not explain in detail which criteria have to be fulfilled to let an event flow into the statistic. Nevertheless, there must have been entered a threshold to filter the events which have a direct impact on people and infrastructure, i.e., a certain degree of severity. Otherwise, the total numbers for all hazards would be far too low.

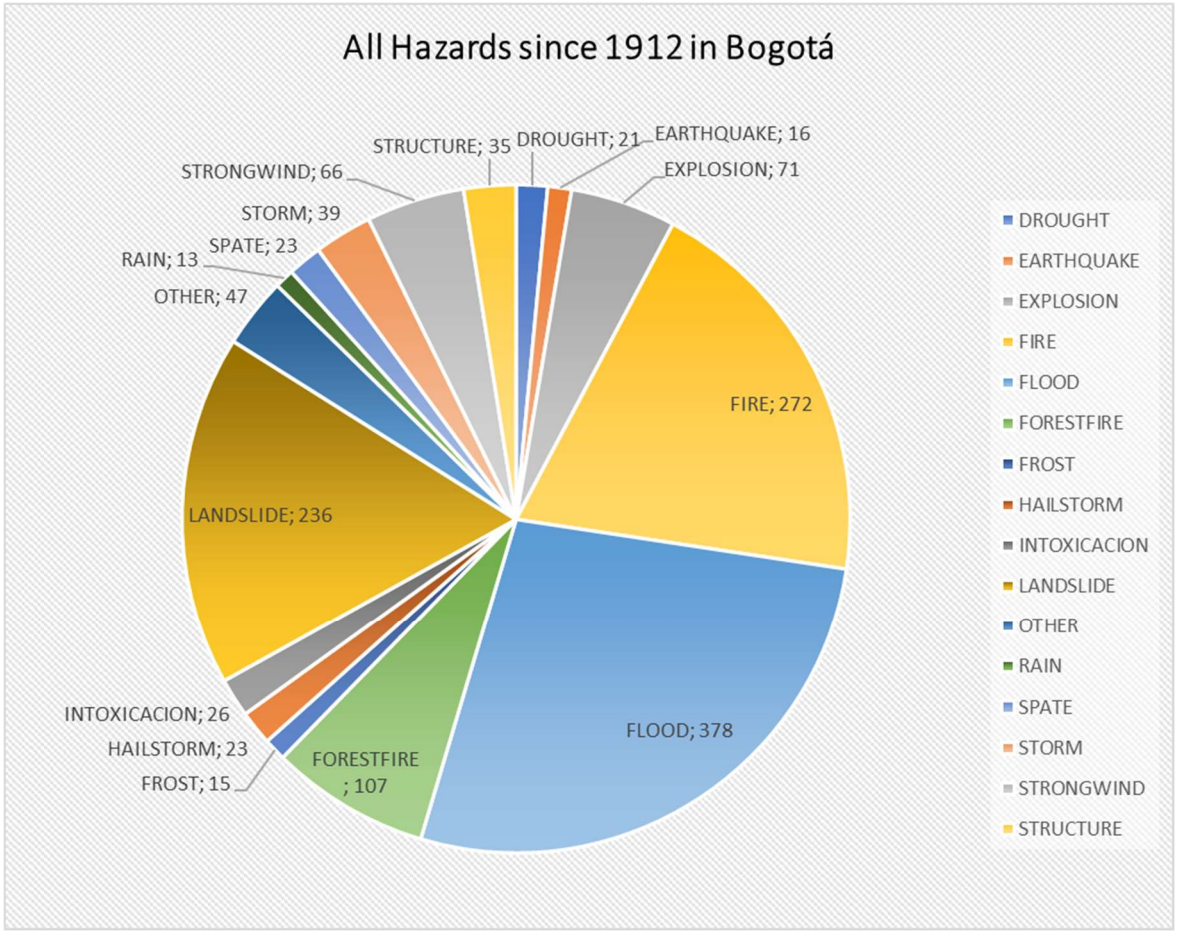

Figure 18: All hazards since 1912 in Bogotá (Desinventar, 2020)

The World Bank Colombia issued a study in 2012 (BancoMundialColombia, 2012) regarding risk management for all natural hazards in Colombia focussing on the duties of the public and private sector to prevent such catastrophes. To understand the impact of the most destructive natural calamities from 1970 to 2011 they put in relation the damages to houses and fatalities they provoke. This statistic is based on data from DANE and for this reason in Spanish language. The shown natural perils are flood,

volcanic activity, earthquake and landslides. On the y-axis are counted the destroyed houses and on the x-axis the people who lost their lives due to one of the occurred hazards.

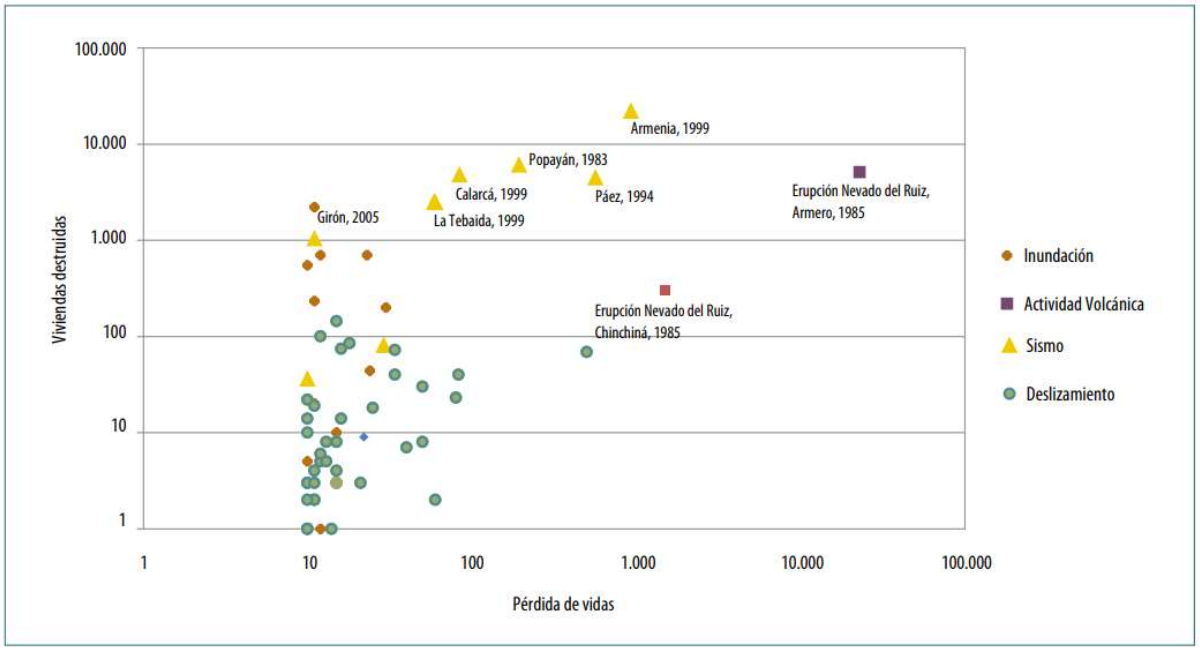

Figure 19: Relation between destroyed houses and fatalities, 1970-2011 (BancoMundialColombia, 2012)

This chart confirms the fact, that there are several very destructive earthquakes that cause thousands of fatalities and have an immense impact on infrastructure bringing wide spread damages. However, in terms of quantity, landslides are the hazard that prevails in Colombia, being aware that in this graphic only the biggest ones are listed.

2.2.1.2. Landslides

The national map of landslide hazard elaborated by the *Servicio Geológico Colombiano* (SGC) shows in a simple way the exposed areas in Colombia. There is a clear dividing line between the eastern and western part of the country, along the Eastern *Cordillera* that goes from South to North. Eastwards of the mountain ranges there is rain forest in the lowland plain with almost no risk to mass movements. The legend of this map describes green areas as a low-risk zone, yellow areas show a medium risk, orange means high risk and red coloured areas represent very high-risk zones. In conclusion, the three Cordilleras are the zone with highest exposure due to its complex terrain and climatic conditions. In the Western Cordillera occur 17% of registered landslides, in the Central Cordillera 43% and in the Eastern Cordillera, including the city of Bogotá, 32% (Aristizábal and Sánchez, 2020). By definition a *landslide* is the movement of a mass of rock, debris, or soil down a slope, under the influence of gravity (Cruden, 1996). In this research the terms landslide and mass movement will be used synonymously.

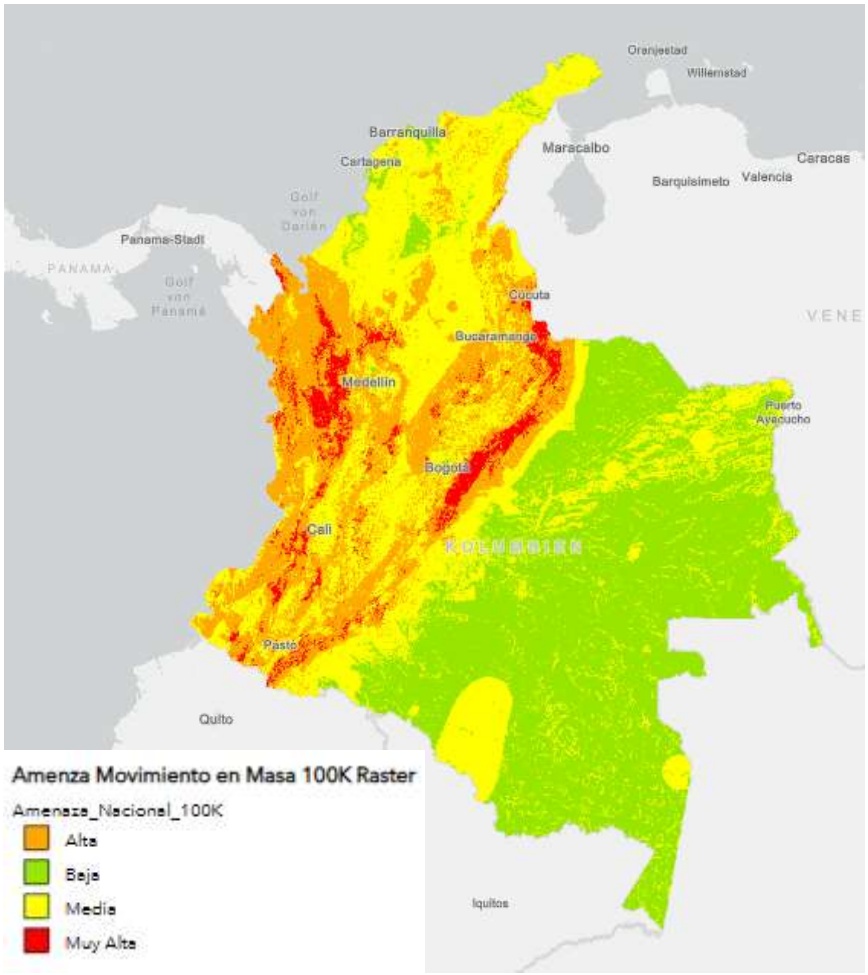

Figure 20: National Map of landslide hazard in Colombia (SGC, 2022)

Between the hazard earthquake and volcanic eruptions on the one hand and on the other hand flood and landslides there can be stated one big difference: The first ones are called invariable hazards, while floodings and landslides belong to variable hazards. Human beings are not in the position to intervene in the dynamics of invariable hazards (BancoMundialColombia, 2012). There are almost no effective measures to protect themselves against these invariable hazards. On the other hand, in respect of variable hazards, preventive and long-term measures can mitigate the risks successfully. (BancoMundialColombia, 2012).

Figure 21 shows the landslides in the whole country Colombia occurred between 1985 and 2017 together with the quantity of affected people, i.e., deaths and injured people, and destroyed houses. Looking at the trendline for the number of landslides, there is a sharp increase of events visible. However, this sole chart cannot explain the concrete reasons for this development. Two factors can influence this evolution: first, the great improvement in reporting and gathering the landslide data and subsequent creation of landslide inventories by governmental and scientific organisations, and second, the increase of population in vulnerable areas that could be affected by the occurrence of a landslide (Aristizábal and Sánchez, 2020). However, the peak of landslides and the peak of damages to infrastructure can be seen in the years 2010 and 2011, coinciding with the phenomenon of La Niña.

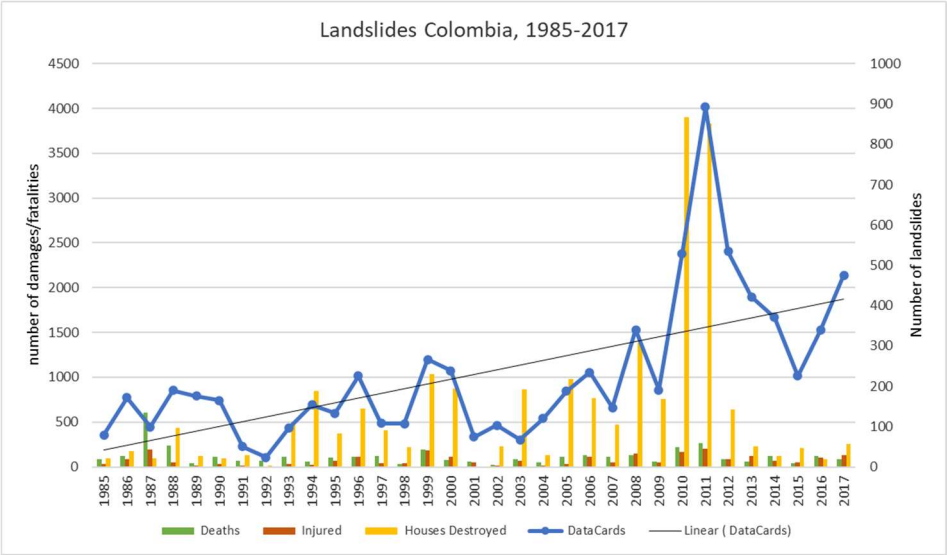

Figure 21: Landslides per year in Colombia and their effect, 1985-2017 (Desinventar, 2020)

Visualising the distribution of number of landslides in Bogotá D.C. it becomes evident that the most exposed districts with the highest numbers of landslides are located in the south of the city. Ciudad Bolivar is outstanding with a total of nearly 1.200 reported landslides between 1996 and 2021. The districts Usme, San Cristóbal and Rafael Uribe Uribe belong to the next category and count between 400 and 650 landslides. The next exposed class with up to 305 landslides, are the districts of the study area. The classes have been created manually to group the districts according to the number of landslides.

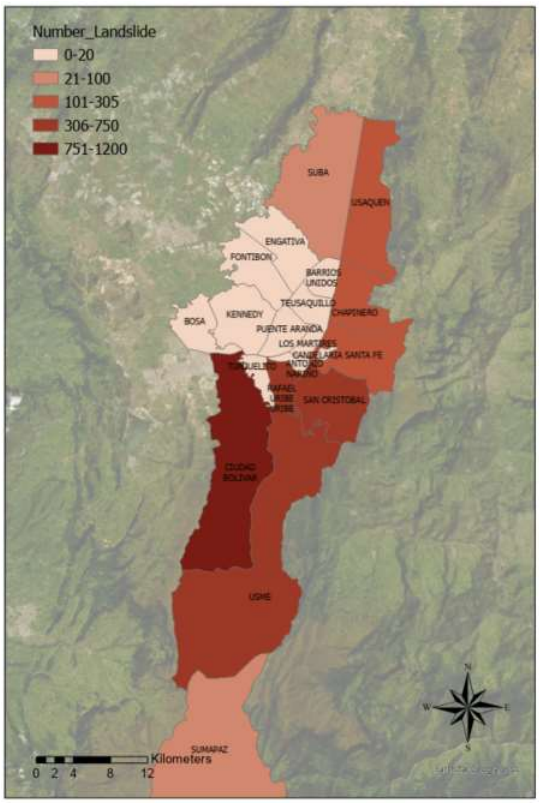

Figure 22: Distribution of landslides in Bogotá, 1996-2021 (IDIGER-4)

2.2.1.3. Types of landslides

To differentiate the type of landslide there are two important approaches: Cruden et al (Cruden, 1996) elaborated a differentiation into five types of mass movements: Fall, Topple, slide, spread and flow. The triggers for the mass movements may be natural ones, such as rainfall, volcanic eruptions or earthquakes or induced by human activity, such as mining, excavation or deforestation.

Understanding the reasons for a mass movement, Cruden et al. distinguish four causative classes: The reasons for the first group are ground-related, these means weak or sensitive materials on the ground. Secondly, morphological causes such as tectonic or volcanic uplift, glacial rebound, fluvial erosion or wave erosion, erosion of the lateral margins and also vegetation removal by forest fire or drought. The third group are physical causes such as intense rainfall, rapid snow melt, prolonged and exceptional precipitations, an earthquake or volcanic eruption, freeze and thaw and shrink and swell weathering. The last group are the man made causes like excavation of the slope, deforestation, irrigation, mining or artificial vibration or water leakage from utilities (Cruden, 1996).

Another, much more detailed approach to distinguish the different types of landslides has been published by Hutchinson in 1988 (Hutchinson, 1988). He classifies mass movements on slopes in eight categories. In this very known paper, Hutchinson does not focus on the trigger elements, but only on very exact description of the movement itself. Among these eight categories can be found category B which are creeps, divided in four subcategories. Category D is landslides, with subcategory of rotational and translational slips. Category E are debris movements of flow-like form and category G are falls, involving fresh detachments of material such es rock and soil falls. There are further categories sagging of mountain slopes, topples and complex slope movements which are not reflected in the IDIGER database. There are neither considered events belonging to category A rebound, i.e., movements triggered by human activity.

The IDIGER mass movement data do not follow exactly one of these categorizations, but are hold in a simpler way rather a mixture of them: There are two outstanding and most frequent categories, namely landslide and debris flow. Creep, rockfall and rotational and translational landslides follow in terms of frequency. It seems that the term landslide is used here as a generic one, while translational and rotational landslide are used for a more detailed description in some cases.

Figure 23 shows the kind of mass movements in Bogotá and the distribution among the single categories.

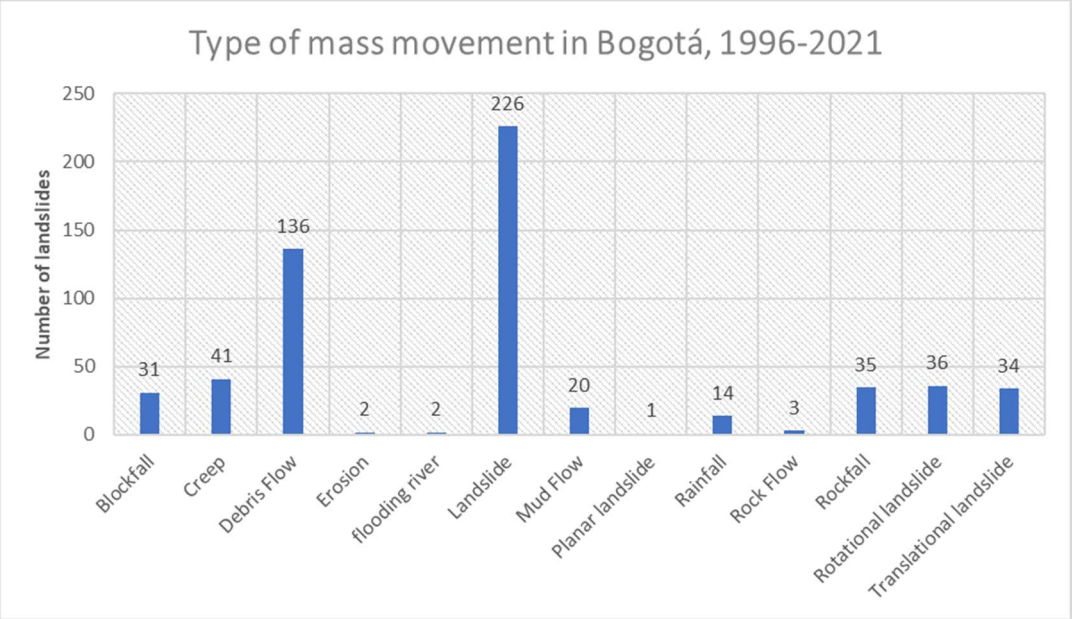

Figure 23: Type of mass movement in Bogotá, 1996-2021 (IDIGER-7)

2.2.1.4. Landslide inventory

The construction of a reliable and meaningful landslide inventory is a challenging task. The most important requirement is the completeness of data, that allows drawing statistical relevant conclusions out of the inventory. The historical events provide useful information about the geographical spread and incidence of landslide events and help to understand where landslides may occur again in the future (Aristizábal and Sánchez, 2020). Completeness of data refers on the one hand to the totality of recorded landslides and on the other hand to the reported parameters of each event.

It has to be assured that there is no double counting of events when combining different sources. This may happen if landslides are not marked unequivocal or if additional visual inspections are carried out. Furthermore, for a reliable basis it should be guaranteed that also smaller landslides enter in the database. However, smaller landslides in remote or inaccessible areas without effects on infrastructure such as houses or roads will probably sometimes not be noticed and do not have any influence on the statistics (Aristizábal and Sánchez, 2020, Abad et al., 2022). Depending on the database, there might be a threshold for inclusion of data to guarantee comparability of the single landslide. It might be helpful to separate small, shallow slope failures with no effect from large to catastrophic landslides that affect broad areas (Kirschbaum et al., 2015).

Important for further analysis, is the correct and exact localisation of the events. Coordinates help to localise the landslide exactly, but in the field work it might be sometimes difficult to gather. The lack of coordinates leads to a very coarse localisation only defined by the road or even only the district. If a landslide is detected to a later point in time the date and cause may be incorrect and lead to a higher degree of inaccuracy of the whole inventory.

Beside the importance of correct localisation of landslides, a sound inventory needs a careful classification regarding type of movement, land cover and material that the movement takes with it. It would be also valuable to know about damages or economic losses. Unfortunately, in reality there is only very few information regarding economic losses caused directly or indirectly by the landslide (Aristizábal and Sánchez, 2020).

The landslide data used in this case study have been provided by the governmental institution IDIGER, *Instituto Distrital de Gestión de Riesgos y Cambio Climático*. This institution which belongs to the mayoralty of Bogotá has the aim to write guidelines for disaster risk management and to find methods to cope with the multiple hazards Bogotá is exposed to. By this way they want to improve the protection of people and guarantee a sustainable development of the city of Bogotá.

Each single landslide stored in the IDIGER database has been reported by inhabitants to local authorities, which send experts to the place where the event occurred to take down all necessary data. This way it should be theoretically granted that every mass movement, at least occurring in the urban areas, is included in the inventory. Nevertheless, looking at the real inventory, the provided information is not complete, mainly regarding its classification. In conclusion it can be said that the incompleteness of data and spatial inaccuracy of mass movement points are the main limitations of the inventories and for the conclusion which can be drawn (Abad et al., 2022).

All point data for the landslide inventory used in this research come from IDIGER. The data have been merged out of three different data collections, which differ in their parameters and localisation level. All point data are projected in MAGNA, WKID 4686 EPSG, also called MAGNA SIRGAS applicable to the country Colombia.

Source	Name	Time frame	Localisation	Data cards	Details
IDIGER	IDIGER - 1	1996-2013	• District • Inner district • Address • coordinates	2.187 for the whole city of Bogotá	• Type of movement • Volume • Slope • type of material • Cause • Cover
IDIGER	IDIGER - 2	2014-2016	• District • Inner district • Address	134 for the whole city of Bogotá	• Type of movement • Volume • Slope • type of material • Cause • Cover
IDIGER	IDIGER - 3	2015-2021	• District • Inner district • Address	1.568 for the whole city of Bogotá	• Type of event • Type of movement • cause • affected infrastructure • affected houses • affected people
IDIGER	IDIGER - 4	1996-2021	• District • Inner district • Address • Partially coordinates	3.885 for the whole city of Bogotá	• IDIGER 1+2+3 combined and corrected
IDIGER	IDIGER - 5, based on IDIGER 1	1996-2013	• District • Inner district • Address • coordinates	464 for the Study area	• Study area: • Usaquén • Chapinero • Santa Fe • Candelaria

IDIGER	IDIGER - 6, based on IDIGER 1+2	1996-2016	• District • Inner district • Address • Partially with coordinates	496 for the Study area	• Study area: • Usaquén • Chapinero • Santa Fe • Candelaria
IDIGER	IDIGER - 7, based on IDIGER 1+2+3	1996-2021	• District • Inner district • Address • Partially with coordinates	867 for the Study area	• Study area: • Usaquén • Chapinero • Santa Fe • Candelaria

Table 4: Landslide inventory 1996-2021 with data provided by IDIGER, own figure

The most accurate database is IDIGER-1, which comes from a shapefile provided by IDIGER with X/Y coordinates for the years 1996-2013.

IDIGER–2 was provided in the same format, but unfortunately, without X/Y coordinates. The data have only been provided only on a more or less accurate address level and are therefore not suitable for accurate visualisation. Nevertheless, the data are suitable for analysis of the landslide parameters.

Data resumed in the file IDIGER-3, which represents the highest number of records in proportion to the number of years, is structured in a completely different way: in this database there is no split regarding cover or type of movement. All records are stored under *risk of movement of mass*, but no further distinction has been made. As in IDIGER–2 the coordinates are missing as well. This inventory concerns more on the damages the landslides trigger. Nevertheless, this inventory is very poor in differentiation within the category values: the category *level of damage* is split up in light, modest, heavy and severe, being about 55% from the total marked with unknown. The same happens to the category *damage to public infrastructure* and *affected houses and families*; around 65% of the records is answered with unknown. Subsequently, no reliable classification of landslides is possible. The idea to focus more on the socioeconomic damage is very valuable, however with scarce and incomplete information the interpretation of data is very difficult.

2.2.2. Land cover

2.2.2.1. Land cover categories

In the following the land cover in the study area shall be examined more in detail. land cover and land cover changes may have a significant influence on the exposure to landslides.

For the analysis of land cover and possible changes, a proper and meaningful classification of satellite images into different categories is essential. In this case study the classification categories will follow the land cover categories of CORINE, belonging to the European Copernicus Land Monitoring Service. I selected the categories that best fit to the environment of Bogotá. The categories will be the same in the four image classifications to allow a better comparison at the end.

The first standardized class are water bodies, normally an easy class to distinguish. There are some water bodies in the area of classification, but this class does not play any role in the study area.

The next two classes describe urban structures: These are continuous urban cover and discontinuous urban cover. Urban cover can be well differentiated from vegetational cover thanks to the spectral characteristics of vegetation used in the relevant band combinations. Discontinuous urban cover can be distinguished from continuous urban cover as there is a lower density of settlements, varying with open spaces and often along big streets. Discontinuous cover can be compared with urban sprawl.

The class bare land is characterized by the fact that in these zones there is no vegetation at all. In this research this may be bare rocks, but also bare soil with no vegetation on it or even areas where a landslide occurred and swept away all vegetation. There are also bare areas in the context of agricultural fields. These areas will be counted to the agricultural class knowing that there might be misunderstandings if no further conditions are defined.

The class forest is used without any further subclasses. Although there are differences in the density of forest, the composition of trees is more or less the same, due to the altitude of the city and the mountains around, the forest belongs to montane forest (Rodríguez et al., 2013).

Agriculture assumes an important paper; Bogotá is surrounded by agricultural areas. Most of them in the northern and north-western part as the topography is very flat there and thanks to the Bogotá River the soil is quite humid and appropriate for crops. The category agricultural areas include pasture and cropland, irrigated and non-irrigated land. Only greenhouses have been assigned an own class, as their spectral characteristics differ a lot from other agricultural areas. Nevertheless, handle greenhouses as a separate class bears the risk of misinterpretation by the programme as they might be recognized as urban fabric or bare land.

On the top of the mountain range there is mainly sparse vegetation, called *Páramos*: this is a vegetational cover without trees and bushland but with robust and low grown plants (Anselm et al., 2018) representing the last category.

ArcGIS Pro offers different classifier to process the land cover classification. In this case study the classifier *support vector machine* has been used. The Support Vector Machine maps the input vector data into a higher dimensional feature space to optimally separate the different classes. Its strengths consist in the ability to handle very large images, it is less susceptible to noises or an unbalanced numbers of training sites within one class (ESRI_ArcGISPro, 2023b).

2.2.2.2. Selection of satellite images

Four satellites images were downloaded from USGS Earth Explorer to carry out a temporal assessment of land cover and land cover change in the study area. On the USGS Earth Explorer site a huge variety of satellite imagery is stored, above all Landsat data from its beginnings until today, publicly available and free of charge. I selected images from the Landsat Serie which belong to the NASA company. To assure a better comparison between the images no picture from another satellite family has been

selected. Of course, there are satellites which provide images with very high resolution such as SPOT 5 or Rapideye, but these images are not freely available and shall not be considered here.

To analyse the images more accurately, mostly cloud-free pictures have been selected in the USGS database. Additionally, I tried to find images that has been taken at the same month or time of the year to compare them correctly.

The first picture out of Landsat 5 is dated at March 30th 1985. The eighties represent a century of uncontrolled growth of the city of Bogotá due to migration pressure. This must be reflected in the comparison of the images afterwards. The second picture is dated on August 30th 1997, also from Landsat 5. This image is taken in August and differs from the other image dates. However, as Bogotá is located in the tropes, seasons are not distinctive as in Western Europe. More important is the consideration of the rainy season months. The third picture out of Landsat 8 dates at January 1st 2014. The time interval of 17 years is quite long, as there was no adequate image in the years before, but this way the pictures from 1997 and 2014 fit perfectly with the years of landslide experience.

The last picture, Landsat 9, is dated January 31st 2022. It should help to understand the current situation in Bogotá regarding Land cover and will also be used as conditioning factor in the subsequent landslide susceptibility mapping.

All images have the same projection and Datum: WGS1984, UTM Zone 18N, Transverse Mercator WKID32618, applicable between 78°W and 72°W.

Accquistion Date	**Optical Sensor/ Data Type**	**Coordinates**	**Number of bands**	**Spectral resolution -bands**	**Spatial Resolution**
1985, March 22nd	Landsat 5, TM_L2SP	Center Lat 4°19’51.10’’N Center Lon 74°28’02.17’’W	7	1 - Blue 2 - Green 3 - Red 4 - Near Infrared (NIR) 5 - Short-wave Infrared (SWIR1) 6 - Thermal Infrared 7 - Short-wave Infrared (SWIR2)	• 30 meters, • 120 meters (thermal)

1997, August 30th	Landsat 5, TM_L2SP	Center Lat 4°19'45.70''N Center Lon 74°27'21.42''W	7	1 - Blue 2 - Green 3 - Red 4 - Near Infrared (NIR) 5 - Short-wave Infrared (SWIR1) 6 - Thermal Infrared 7 - Short-wave Infrared (SWIR2)	• 30 meters, • 120 meters (thermal)
2014, January 1st	Landsat 8, OLI_TIRS_ L2SP	Center Lat 5°47'06.04''N Center Lon 74°10'36.91''W	11	1 - Coastal 2 - Blue 3 - Green 4 - Red 5- NIR1 6 - SWIR-1 7 - SWIR-2 8 -Panchromatic 9 - Cirrus, 10 - TIRS-1 11 - TIRS-2	• 15 meters (panch-romatic) • 30 meters • 100 meters (TIR)
2022, January 31st	Landsat 9, OLI_TIRS_ L2SP	Center Lat 4°20'21.48''N Center Lon 74°29'14.06''W	11	1 - Coastal, 2 - Blue 3 - Green, 4 - Red 5- NIR1 6 - SWIR-1 7 - SWIR-2 8 - Panchromatic 9 - Cirrus 10 - TIRS-1, 11 - TIRS-2	• 15 meters (panch-romatic) • 30 meters • 100 meters (TIR)

Table 5: Satellite images used for land cover classification, own figure

To proceed with the analysis, only a part of the total satellite image, namely the conurbation of Bogotá including the study area has been selected, an area of about 1.360 km^2.

Figures 24-27 show the four Landsat images that are to be classified in a false colour optic to stress the vegetational cover in red colours.

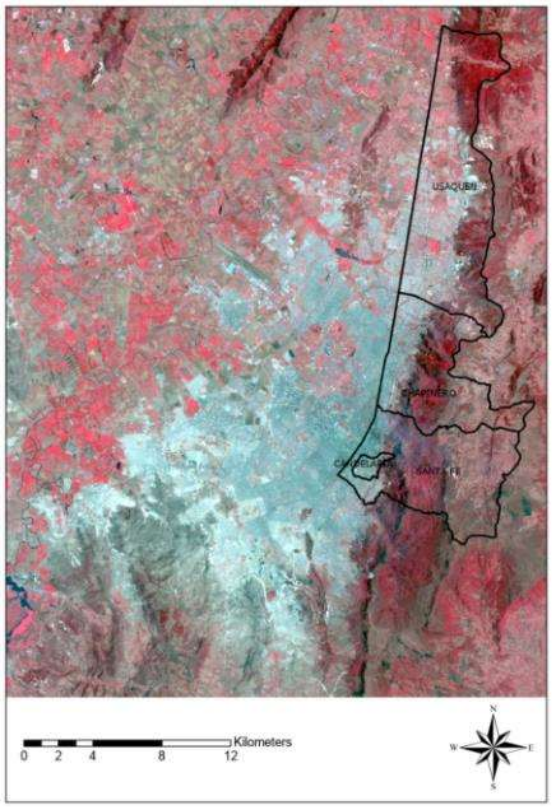

Figure 24: Landsat 5 image, 1985, in false colour optic

Figure 25: Landsat 5 image, 1997, in false colour optic

Figure 26: Landsat 8 image, 2014, in false colour optic

Figure 27: Landsat 9 image, 2022, in false colour optic

2.2.2.3. Supervised Classification

Landsat 5, holds 7 and Landsat 8 and 9 hold 11 spectral bands which can be combined in various ways to make different aspects of the imagery visible. In this study the thermal bands are not used, the focus lies on the bands 1-8 and in Landsat 5 on the bands 1-5. The most important combination to distinguish vegetation from areas without vegetation is the false colour image, in Landsat 5 this is the band combination 4-3-2, in Landsat 8/ 9 5-4-3. Applying this combination, vegetation appears in red colours, urban cover or bare soil appear in different shades of grey, meaning that there is no vegetation at all. For sparsely vegetated areas or fields in different vegetational stages, there may be every nuance of red in between.

Beside the false colour view, I used frequently the combination 7-6-4 (in Landsat 8/9, in Landsat 5: 6-5-3) which shows vegetation in different shades of green depending on how healthy vegetation is. A further useful combination was 6-5-2 (Landsat 8/9, Landsat 5: 5-4-1), specific for agriculture. Selecting these spectral band combinations, crops appear in green, bare areas in magenta and non-crop areas are coloured in subdue green.

Object-based image analysis (OBIA) consists of two important steps, segmentation and classification, followed by an accuracy assessment at the end to check the reliability of the outcome (Amatya et al., 2021). The first step in all four images is the automatic segmentation done by ArcGIS Pro. The segmentation tool combines pixel of same spectral characteristics to objects that appear in the same colour. There are three parameters to adapt for the own purposes: Spectral detail (default 15,5), spatial detail (default 15) and minimum segment size in pixels (default 15) which I reduced in all cases to seven7 to make also smaller elements visible. As the pixel size is 30 m x 30 m, I considered this reduction necessary for a reliable result. The segmentation step has been processed on the basis of the false colour image to maintain the split of vegetational covers and zones without vegetation.

In this research the method of supervised classification will be applied and therefore the second, more extensive, step is the collection of training samples doing manually for all four images by contributing a category to every group of pixels. This step has to be done very precisely as this presents the basis of the following automatic OBIA classification step. In respect of the classification itself, it is essential to have enough samples per class to allow a proper classification process. In this study there have been selected between 20 and 30 samples per class.

To facilitate the decision to which category every object belongs, I used as a supporting tool Google Earth satellite view for the different years to crosscheck the land cover classification. The resolution of the Google Earth images for the last years is very high, so it is a suitable tool for the years 2022 and 2014. The number of images in the eighties is limited and the resolution rather coarse, they are therefore only of restricted use for the decision process.

Another way to identify the land cover is the Normalized difference vegetation index (NDVI). This index, that ranges between -1 for no vegetation an +1 for dense and healthy vegetational cover, results out of a calculation of spectral bands from the satellite images. The NDVI is the normalized difference between the red and the infrared band: NDVI = (NIR – Red) / (NIR + Red). For a better visualization the

colour ramp goes from red to green to understand if an area is covered with vegetation or where soil sealing and bare land prevail (in red and orange). However, the benefit of this index is sometimes limited, mainly in mountainous regions with high slopes where the camera angle is not optimal. Figure 28 illustrates the NDVI for the study area for the year 2022 where the mountain range appears in orange and yellow colours what would signify that there is no vegetation.

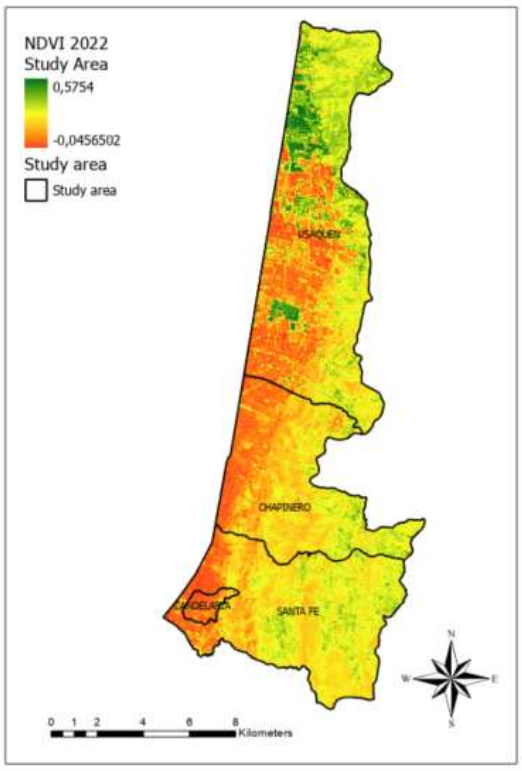

Figure 28: NDVI 2022

Images with clouds have been avoided, however in the image of 2014 there are some smaller clouds above of the relevant area. The percentage is only about 4%, nevertheless the clouds and their shadows hide the real land cover classes. After the process of segmentation and classification some cloud pixels have been removed and reclassified manually, verified with the surrounding classes and the underlying Landsat image.

The surroundings of Bogotá are in some cases quite challenging to classify as the land cover is often very fragmented, with entities that look like a mosaic: Above all the extensive agricultural zones that clash with urban cover, forest and shrubland are sometimes difficult to distinguish.

The accuracy assessment terminates the process of classification by spreading randomly points over the classified area with the aim to be crosschecked if they have been contributed to the correct category. After the whole process of supervised classification, the raster outcome will be extracted to the size of the study area and also transformed to a vector file with polygons to work more easily on it and to compare size and changes in the single classes.

2.2.3. Creation of Susceptibiliy Map

2.2.3.1. Likelihood Frequency Ratio approach

Landslide susceptibility is defined by a quantitative or qualitative assessment of the classification, volume and spatial distribution of landslides which exist or potentially may occur in an area (Lee and Ab Talib, 2005). To calculate the Landslide Susceptibility Index (LSI) two approaches can be roughly divided: the heuristically based and the statistically based one (Goyes-Peñafiel and Hernandez-Rojas, 2021). Among the statistical methods, there are bivariate and multivariate methods. In the bivariate statistical approach, each conditioning factor is overlaid with the landslide inventory map and weighting values based on the landslide densities per each factor class (Akgun et al., 2008). To this method belong the Weights of Evidence approach and the Likelihood Frequency Ratio (FR). However, in the bivariate statistics no relationships between the single geo-environmental factors can be considered. Multivariate statistical techniques such as Logistic Regression take into account dependencies and collinearity between some factors (Goyes-Peñafiel and Hernandez-Rojas, 2021).

The Likelihood Frequency Ratio approach is one of the probability models based on the observed relationship between the distribution of landslides and each landslide-related factor (Solaimani et al., 2012). The aim is to reveal the correlation between past landslide locations and a set of selected geo-environmental factors using the calculated frequency ratio of each category (Lee, 2005, Ramesh and Anbazhagan, 2014). For the calculation of the frequency ratio the landslide database IDIGER 5 has been used, i.e., 464 landslides.

The frequency ratio is the landslide ratio divided by the class ratio. The landslide ratio is the number of landslides in pixel in a certain class (a) divided by the total number of landslides (A), i.e., 464 in this study. The class ratio is calculated by dividing all pixels belonging to a certain class (b) divided by the total number of pixels in the study area (B). If the resulting frequency ratio is greater than 1, it means a higher correlation and a higher probability of a landslide, while a ratio below 1 means a lower correlation and subsequently a lower probability of a landslide (Lee, 2005). The formula for this approach is:

$$FR = (a/A) / (b/B)$$

For this calculation, the set of geo-environmental factors was first converted into raster format, in the case of land cover, geological categories, buffer drainage system and buffer geological faults. The raster data have than be resampled to the same cell size (30m) and the same projection (MAGNA, WKID 4686) to guarantee no false overlaps of layers. In the case of the land cover map the projection WGS1984 18N has been maintained as a conversion was not possible.

In the next step the layers with continuous data, these are the DEM, slope, TWI and plan and profile curvature have been reclassified in equal intervals summarizing the values to classes. For each of these classes the percentage of landslides was calculated, i.e., the landslide density per class. In a second reclassification, step every class has been assigned the individual frequency ratio to weight the classes within their respective conditioning factor or category.

The Landslide Susceptibility Index (LSI) is the final value which is presented in the susceptibility map.

In the calculation of susceptibility, each category will be multiplied with the sum of frequency ratios of all classes. Subsequently, each pixel will have an associated LSI (Goyes-Peñafiel and Hernandez-Rojas, 2021) to measure the degree of susceptibility at any point of the study area.

$LSI = FR_1 + FR_2 + \ldots + FR_n$, where FR is the rating of each factor´s type of range (Lee, 2005) and *n* the number of selected conditioning factors.

$$\sum FR\,n$$

The LSI can range from 0 to infinity, the higher the LSI value, the higher the landslide susceptibility is in this point as there are higher frequency ratio of single classes multiplied.

2.2.3.2. Conditioning factors

In general, it is assumed that landslide occurrence is determined by conditioning factors and that future landslides will occur under the same conditions as in the past (Lee and Ab Talib, 2005). Landslide susceptibility saps describe the spatial distribution of the landslide probability in a given area based on local geo-environmental factors. These geo-environmental factors are not binding, they can be chosen among different factors that seem appropriate for the particular area (Aristizábal et al., 2019). However, most scientific studies use similar factors, mainly DEM-derived raster data such as slope, aspect and curvature (Abad et al., 2022, Goyes-Peñafiel and Hernandez-Rojas, 2021, Akgun et al., 2008).

Depending on the literature, there are different numbers of factors used for the creation of the map. In this research 10 conditioning parameters will be used for calculation of susceptibility. The factors can be divided into three thematic origins (table 6): The first one is the group of terrain derivatives. The DEM is the basis data, out of which the following factors have been derived: Slope, slope aspect, plan curvature, profile curvature and the Topographic Wetness Index (TWI). The second group are the landscape factors, to which belong the elaborated land cover categories and the distance to water courses, in this case the drainage system. The third group are geological factors, these include the distance to geological faults and the relevant geological categories.

The susceptibility map should reflect the most recent situation. However, the acquisition dates of the conditioning factors are not exactly the same, which should not affect the result. While all the factors derived from the DEM can only be dated between 2000 and 2013, the geological classes (IDECA, 2022b) have been updated in 2019 and the distance to drainage (IDECA, 2022a) in 2021. The data on distance to faults have been created in 2018 (IDIGER, 2018). These factors are not subject to a high degree of variability and should therefore be stable in the medium-term view.

For the conditioning factor land cover, the Landsat image from 2022 was used to show the most recent situation. Land cover could be the most changeable category with an impact on the result on the susceptibility result.

The basis for the calculation of the frequency ratio per class is the landslide inventory IDIGER 5, namely the data with XY coordinates from 1996 to 2013.

DEM: The Digital Elevation Modell (DEM) is indispensable for any topographic analysis as it serves as a visual overview how the grading of altitudes looks like in a certain region. The used DEM is called Terra Advanced Spaceborne Thermal Emission and Reflection Radiometer (ASTER) Global Digital Elevation Modell (GDEM) Version 3 (ASTGTM v003) from NASA which has been downloaded from the USGS Earth Explorer (USGS_Earth_Explorer, 2013). The acquisition date stated in the USGS homepage is between 2000 and 2013, there is not given any exacter date.

The DEM has a spatial resolution of 1 arc second (1x1 degree tiles, what is approximately 30 meter). Two of these DEM have been used and merged in ArcGIS Pro to cover the whole region of Bogotá

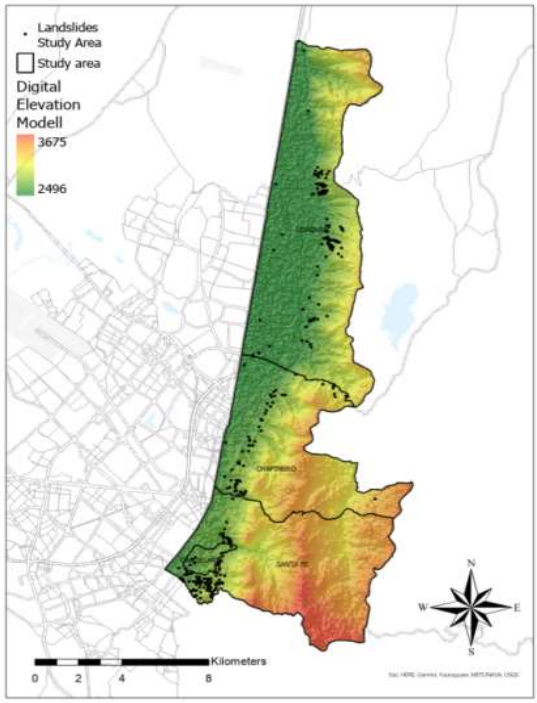

Figure 29: DEM with underlying hillshade and landslides (IDIGER-5)

The altitude of a point is an important parameter which must be considered in the calculation of susceptibility. The study area is located between 2.500m and roughly 3.700m. About 30% belongs to the lowest class. The next 30% belong to the altitudes from 2.600 until 3.000m. The last 35% go from 3.000 to 3.300m. Only 5% belong to the highest zones up to 3.700m.

Slope: The slope represents the steepness of the terrain. The value range is from 0 degree to 90 degree. In this study area the highest degree is 72% and the total range has been divided in equal intervals. The steepest slopes can be found in Santa Fe, in the zones bordering to the city. However, these high slopes represent only 0,40% of the total area. The lower degrees up to 24% slope represent about 85% of the total region.

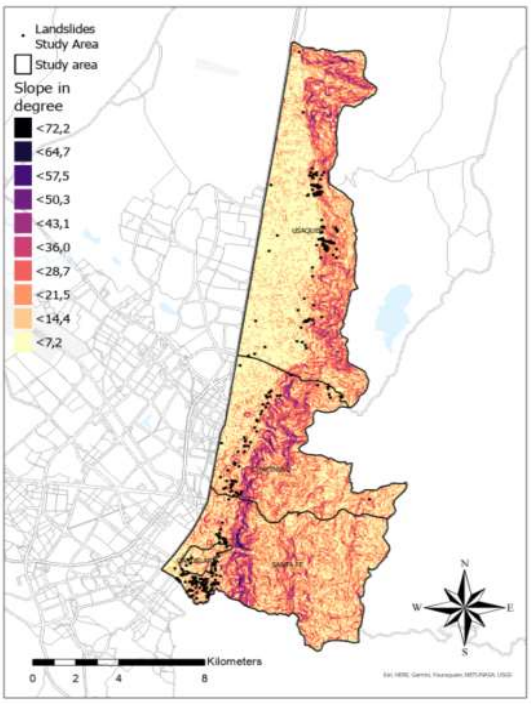

Figure 30: Slope in the study area

Slope aspect: Slope aspect means the orientation of the hills. It is divided into eight directional classes from North, Northeast, East, Southeast, South, Southwest, West and Northwest. In this case the majority of slopes, above all the slopes along the urban area, is oriented towards the Southwest, Northwest and West (55%). In the eastern area of Santa Fe there is also a more yellow and turquoise coloured zone, which means orientation towards the West and South.

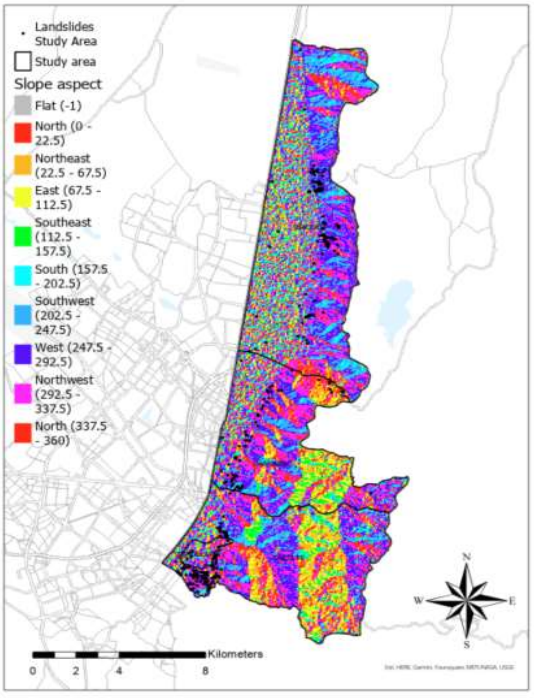

Figure 31: Slope aspect with landslides

Curvature: The curvature values represent the morphology of topography; the more positive or negative the value of curvature is, the higher the probability of a landslide. A positive curvature value indicates convex structure at this grid. A negative curvature indicates a concave surface at this grid (Lee and Ab Talib, 2005). A curvature value of 0 indicates a flat surface. The explication for this behaviour is the fact that convex and concave contours can keep more water after rainfalls, what can increase the probability of a landslide. There are two subgroups of curvature, plan and profile which describe different formations of the surface.

Curvature plan: Plan curvature is perpendicular to the direction of the slope and relates to the convergence or divergence of the mass movement across a surface, but not the acceleration or deceleration of the movement. A positive value indicates that the surface is laterally convex this point, a negative value indicates a laterally concave point. A value of zero indicates a linear surface (ESRI_ArcGISPro, 2023a).

Curvature profile: Profile curvature is parallel to the slope and indicates the direction of maximum slope. It affects the acceleration of mass movements across the surface. A negative value indicates that the surface is convex at that point and the flow will be decelerated. A positive value indicates that the surface is concave at this point and that the flow will be accelerated. A value of zero indicates that the surface is linear without curvature (ESRI_ArcGISPro, 2023a).

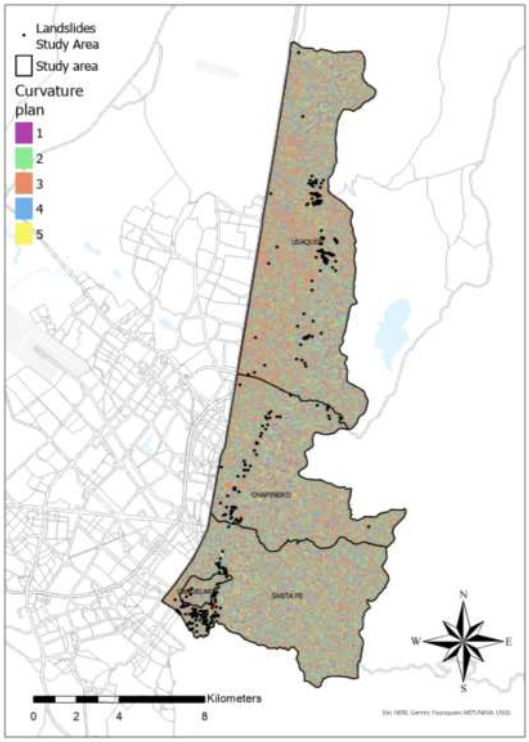

Figure 32: Curvature plan with landslides

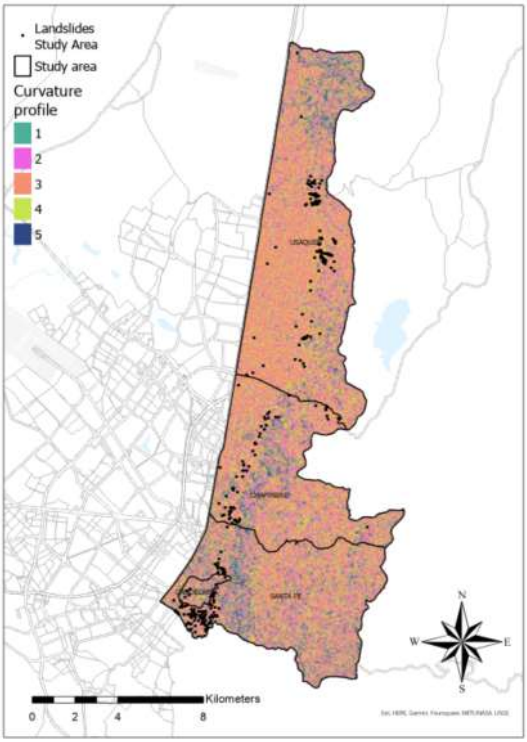

Figure 33: Curvature profile with landslides

The Topographic Wetness Index (TWI) is commonly used to quantify topographic influence on hydrological processes, it quantifies terrain driven variation in soil moisture. The TWI combines the water supply from the catchment area upslope and the downslope water drainage for each cell of a

DEM (Kopecký et al., 2020). The TWI is therefore an important factor to be included in the susceptibility map.

Soil moisture is an important factor for environmental processes but difficult to measure and above all to interpolate across space. A possibility consists in derive the TWI from a digital elevation model (Kopecký et al., 2020), method that will be used in this study as well.

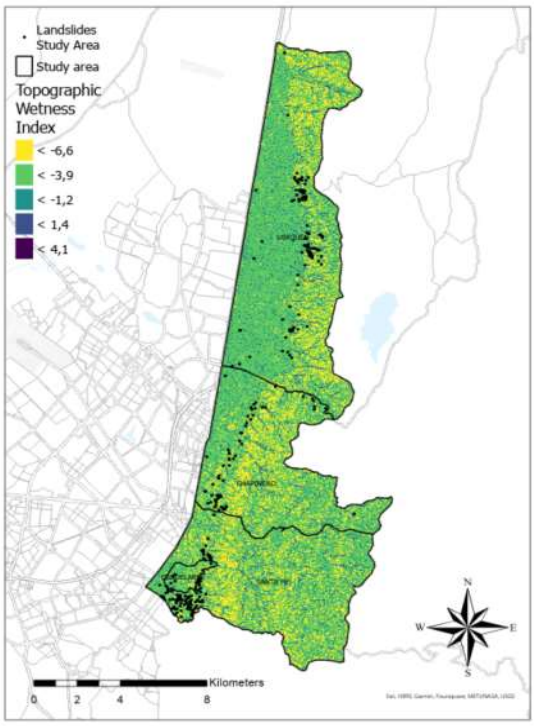

Figure 34: Topographic Wetness Index with landslides

In ArcGIS Pro the calculation process is the following: The basis is the Digital Elevation Model with a resolution of 27m (cell size 0,0002777). The first step is the calculation of the Flow direction. The Flow direction is used to process the next step called Flow Accumulation. The Slope in degree is calculated from the Digital Elevation Modell. These are the three ingredients for the following calculation of TWI.

The slope in degree out of the DEM will be multiplied with 1.570796 and the product divided by 90 to convert slope in degree in radians. Then, the tangents of this converted slope will be calculated.

The result of Flow accumulation (from the beginning) is multiplied with the cell size of original DEM, in this case 0.0002777m to receive the Scaled Flow Accumulation. The real wetness index is the logarithm (Ln) from the Scaled Flow Accumulation divided by the tangents of the slope.

In the final visual result, the wetness of the soil is visible, and water courses are coloured in blue. Resuming the TWI = ln (Flow Accumulation * cell size of DEM)/ tan Slope.

Actually, the TWI is unitless, but, high values indicate a high potential for saturation of soils and low values indicate low potential for saturation. In a consequence, grid cells with the same TWI provide the same hydrological response (USGS, 2007).

Land cover: for the susceptibility map the situation of land cover in January 2022 will be included. Depending on the category of land cover, the probability of a mass movement varies significantly. It is evident, that the majority of landslides occurs in zones with urban cover, or with a pronounced anthropogenic character. The areas covered with forests or denser vegetation are not affected significantly by landslides.

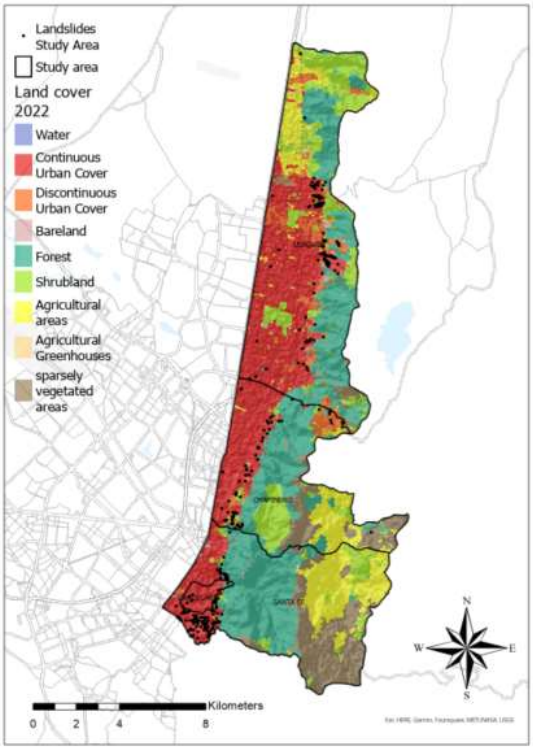

Figure 35: Land cover 2022 with underlying hillshade and landslides

Distance to Drainage: following the literature (Abad et al., 2022, Akgun et al., 2008, Tešić et al., 2020) I chose the same starting point for multiring buffering 50m, going up to 1500m to catch up the landslide that are most distant. The distances differ from research area to research area due to the different topographical conditions and size of study area. The water of the drainage system is one of the main sources of soil moisture (Tešić et al., 2020). About 30% of the study area is located nearer than 100m to a drainage canal.

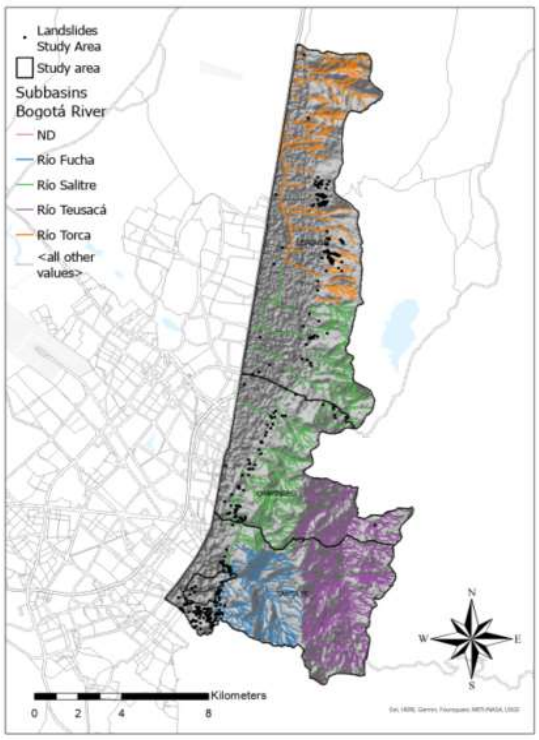

Figure 36: Drainage system with hillshade and landslides

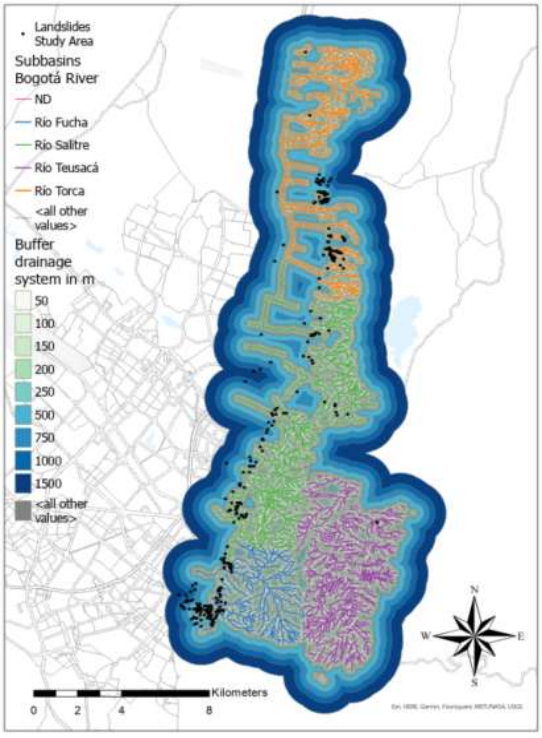

Figure 37: Drainage system with buffering

Distance to faults: Fault lines usually break rock mass structure and reduce their strength. In topographic complex areas, landslides often occur in proximity to these faults (Liu et al., 2022). The buffering for the distance to fault lines have been made similar to the distance to drainage, starting at 50m and going up to 2.000m.

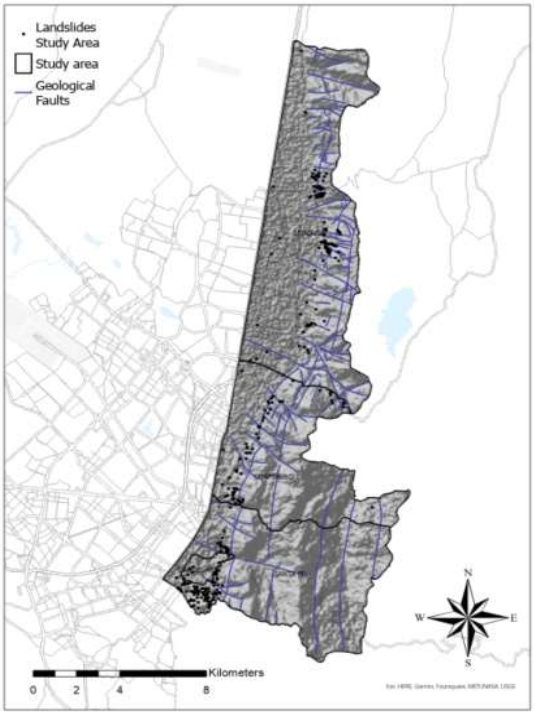

Figure 38: Geological faults with hillshade and landslides

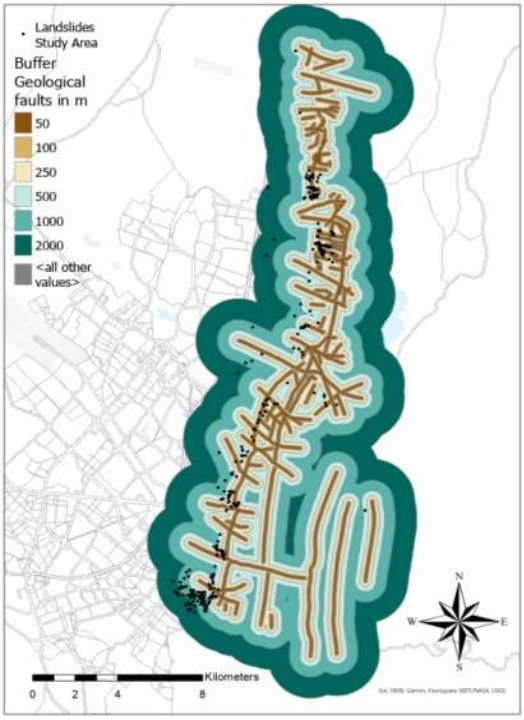

Figure 39: Geological faults with buffering

Geology: The 19 different geological classes have been grouped into five. These are alluvium, clay, deposits, limestone and sandstone. Sandstone represents almost 40% and can be found along the slopes from south to the north. Clay is predominant at the level below the urban cover and in the mountainous area and represents almost the half (48%) of the total ground in the study area.

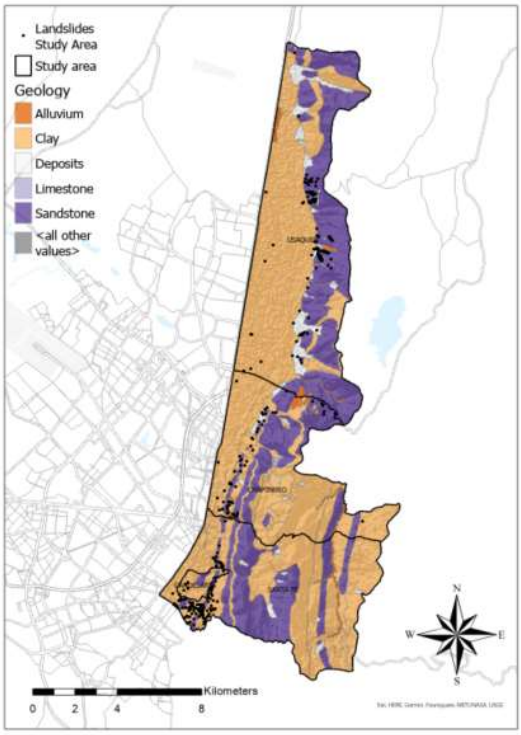

Figure 40: Geological categories with underlying hillshade and landslides

Thematic origin	Parameter	Class	Reclassification	Pixel per class	percentage of class	Number of landslides	density of landslides	Frequency ratio
Terrain derivatives	**DEM**	2.496-2.613m	1	46930	29,51%	113	24,35%	0,83
		2.613-2.731m	2	19370	12,18%	255	54,96%	4,51
		2.731-2.849m	3	14130	8,88%	81	17,46%	1,96
		2.849-2.967m	4	14112	8,87%	6	1,29%	0,15
		2.967-3.085m	5	19698	12,39%	7	1,51%	0,12
		3.085-3.203m	6	18665	11,74%	2	0,43%	0,04
		3.203-3.321m	7	17946	11,28%	0	0,00%	0,00
		3.321-3.439m	8	5207	3,27%	0	0,00%	0,00
		3.439-3.557m	9	2567	1,61%	0	0,00%	0,00
		3.557-3.675m	10	411	0,26%	0	0,00%	0,00
	Total			159.036		464		**7,61**
	Slope	0-5,37	1	28353	18,14%	64	13,79%	0,76
		5,38-9,89	2	34638	22,16%	93	20,04%	0,90
		9,90-14,4	3	29382	18,80%	85	18,32%	0,97
		14,5-18,9	4	22621	14,47%	89	19,18%	1,33
		19-23,4	5	16266	10,41%	68	14,66%	1,41
		23,5-28,2	6	10978	7,02%	40	8,62%	1,23
		28,3-33,3	7	6849	4,38%	24	5,17%	1,18
		33,4-39,3	8	4399	2,81%	1	0,22%	0,08
		39,4-47,2	9	2179	1,39%	0	0,00%	0,00
		47,3-72	10	623	0,40%	0	0,00%	0,00
	Total			156.288		464		**7,86**
	Aspect	Flat	1					
		North (0-22,5)	2	10360	6,29%	20	4,31%	0,68
		Northeast (22.5-67.5)	3	17664	10,73%	20	4,31%	0,40
		East (67.5-112.5)	4	13191	8,01%	15	3,23%	0,40
		Southeast (112.5-157.5)	5	10122	6,15%	7	1,51%	0,25
		South (157.5-202.5)	6	11845	7,20%	21	4,53%	0,63
		Southwest (202.5-247.5)	7	23847	14,49%	75	16,16%	1,12
		West (247.5-292.5)	8	35137	21,35%	177	38,15%	1,79
		Northwest (292.5-337.5)	9	31178	18,94%	96	20,69%	1,09
		North (337.5-360)	10	11254	6,84%	33	7,11%	1,04
	Total			164.598		464		**7,40**
	Plan curvature	unitless	1	9052	5,69%	14	3,02%	0,53
			2	36351	22,86%	132	28,45%	1,24
			3	64493	40,55%	195	42,03%	1,04
			4	38186	24,01%	112	24,14%	1,01
			5	10954	6,89%	11	2,37%	0,34
	Total			159.036		464		**4,16**
	profile curvature	unitless	1	8025	4,78%	11	2,37%	0,50
			2	36846	21,95%	79	17,03%	0,78
			3	64274	38,29%	211	45,47%	1,19
			4	48136	28,67%	117	25,22%	0,88
			5	10591	6,31%	46	9,91%	1,57
	Total			167.872		464		**4,91**
	TWI	unitless	1	34596	21,02%	93	20,04%	0,95
			2	105936	64,36%	284	61,21%	0,95
			3	20987	12,75%	65	14,01%	1,10
			4	3013	1,83%	22	4,74%	2,59
			5	66	0,04%	0	0,00%	0,00
	Total			164.598		464		**5,59**

Thematic origin	Parameter	Class	Reclassification	Pixel per class	percentage of class	Number of landslides	density of landslides	Frequency ratio
Landscape factors	**Land Cover**	Water	1	44	0,03%	0	0,00%	0,00
		Continuous Urban Cover	2	46601	27,87%	370	79,74%	2,86
		Discontinuous Urban Cover	3	8404	5,03%	42	9,05%	1,80
		Bareland	4	612	0,37%	0	0,00%	0,00
		Forest	5	49138	29,38%	36	7,76%	0,26
		Shrubland	6	21773	13,02%	13	2,80%	0,22
		Agricultural areas	7	20395	12,20%	1	0,22%	0,02
		Agricultural Greenhouses	8	531	0,32%	0	0,00%	0,00
		sparsely vegetated areas	9	19733	11,80%	2	0,43%	0,04
	Total			167.231		464		**5,20**
	Distance to drainage							
		0-50m	1	48576	18,05%	98	21,12%	1,17
		50-100m	2	34273	12,73%	73	15,73%	1,24
		100-150m	3	21700	8,06%	46	9,91%	1,23
		150-200m	4	14658	5,45%	31	6,68%	1,23
		200-250m	5	11108	4,13%	35	7,54%	1,83
		250-500m	6	38685	14,37%	135	29,09%	2,02
		500-750m	7	27619	10,26%	23	4,96%	0,48
		750-1000m	8	24743	9,19%	18	3,88%	0,42
		1000-1500m	9	47830	17,77%	5	1,08%	0,06
	Total			269.192		464		**9,68**
Geological factors	**Distance to faults**							
		0-50m	1	18112	6,14%	53	11,42%	1,86
		50-100m	2	17341	5,87%	68	14,66%	2,49
		100-250m	3	42714	14,47%	107	23,06%	1,59
		250-500m	4	51362	17,40%	107	23,06%	1,33
		500-1000m	5	66970	22,69%	91	19,61%	0,86
		1000-2000m	6	98686	33,43%	38	8,19%	0,24
	Total			295.185		464		**8,38**
	Geology	Alluvium	1	2296	1,36%	9	1,94%	1,43
		Clay	2	105707	62,31%	225	48,49%	0,78
		Deposits	3	5949	3,52%	49	10,56%	3,00
		Limestone	4	170	0,10%	0	0,00%	0,00
		Sandstone	5	55342	32,71%	181	39,01%	1,19
	Total			169.464		464		**6,40**

Table 6: Conditioning Factors with corresponding frequency ratio, own figure

To calculate the LSI, the ten conditioning factors must be multiplied by the corresponding frequency ratio. This was done using the raster calculator. The result is an index for each point in the study area

LSI= DEM*7,61 + Slope*7,86 + Aspect*7,40 + Plan Curvature*4,16 + Profile Curvature*4,91 + TWI*5,59 + Land cover*5,20 + Distance to drainage*9,68 + Distance to faults*8,38 + Geology*6,40

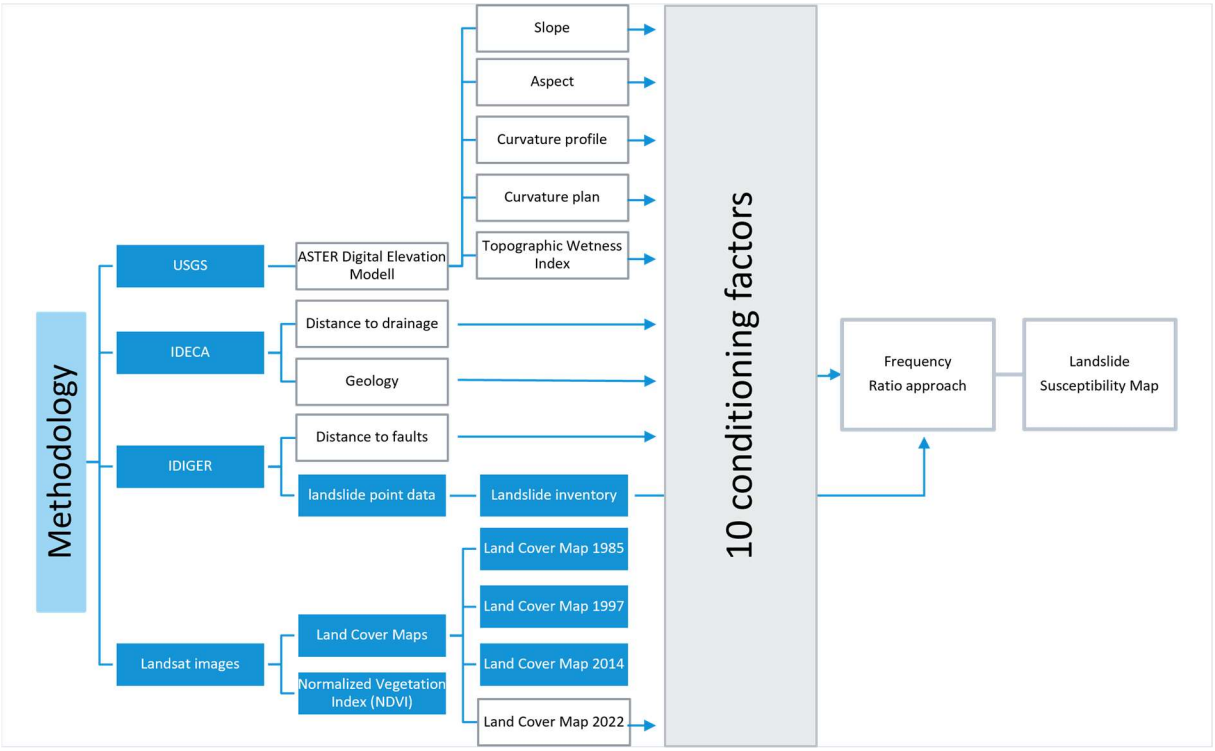

Figure 41: Methodology conditioning factors, own figure

3. Results and Discussion

3.1. Challenges in land cover classification

In the automatic process of segmentation, the minimum size of an object was determined to seven pixels. Therefore, no smaller objects are considered and will not appear in the final segmented image. They can neither be used in the following classification process nor in the image comparison. However, a too high resolution in segmentation would mean a too detailed classified image which is not necessary for the goal of observing rather big developments

The 30-metre resolution of the Landsat images used is satisfactory for ecosystems with little variation. In this case, the surroundings of Bogotá are highly fragmented and show topographically complex mosaics of different land covers and land uses. In addition, the steep slopes in some parts of the study area make it difficult to identify the correct land cover, as shadows make the ground appear very dark.

After several rounds of classification, improving the selection of training samples and reclassifying pixel-wise incorrectly assigned classes, the limitations of this type of supervised classification become apparent. Without implementing further conditions on how the decision to assign a class should be made, the programme relies only on the spectral characteristics of a segmented entity. This is not always sufficient and it would be helpful to consider the shape of an entity or its location

However, without any further conditioning it is possible to do a reliable split of urban cover and different covers of vegetation, such as forest, agricultural areas and sparsely vegetated zones. The goal of the research is more to see tendencies of developments and land cover changes, than examine pixel by pixel what kind of changes might have been occurred.

A challenge with greater impact on the supervised classification process are the high slopes in the east of the city. Here the backscatter of wavelengths seems to be difficult, with the consequence that some areas appear darker and sometimes not in red colours, even though it is about densely vegetated areas. Taking the NDVI as a supportive tool to examine the vegetational cover and to draw conclusions of how healthy and green the vegetation is, the results are insufficient: the western aspects of the slopes appear in yellow and orange colours, which would mean that there is no vegetation at all or vegetation with very little chlorophyll, i.e., less healthy vegetation (figure 28).

The NDVI is a helpful indicator but more in plane areas, such as agricultural zones. Agricultural zones are characterized by small scale rectangles that are side by side. Agriculture can be found above all in the north of the study area and in the east of the mountain range in Santa Fe. Crops are not all in the same point of the vegetational cycle, they grow at different time points during the year. Therefore, some fields appear in clear green colours (analysed with the support of NDVI), other in red or orange meaning that there is no crop at all at this moment. Some fields are only covered with grassland that might be healthy or very dry. So, the automatic classification may lead to misinterpretations of the agricultural areas due to the variety of states.

Some further distinctions are difficult to make: bare lands and urban cover may have the same spectral characteristics and are not recognized by the programme correctly. The difference between

greenhouses in agricultural areas and roofs in the city is also not always clearly distinguishable as both reflect almost all wavelengths and appear nearly white in the false colour image. These misinterpretations have been removed manually afterwards.

3.1.1. Results of Accuracy Assessment

Scientific research always requests a validation of the results to prove their reliability. In the case of land cover classification an accuracy assessment has been made. Hereby a number of points (200) has been randomly spread over the study area. The attribute table shows the underlying class which has to be confirmed or corrected. The result is a table which puts in relation the correct percentual assignation of a class by the user and by the programme. The final kappa coefficient indicates the level of correctness of classification. The values go from 0% to 100%, what would mean a complete correct classification on the basis of these random points. However, the reasons for the level of the kappa coefficient have to be understood well. Sometimes one or two classes bring very weak assignation rates and this leads to a lower overall result. Kappa represents always the average between all correct and incorrect assignations.

Value of Kappa	Level of Agreement	% of Data that are Reliable
0–.20	None	0–4%
.21–.39	Minimal	4–15%
.40–.59	Weak	15–35%
.60–.79	Moderate	35–63%
.80–.90	Strong	64–81%
Above.90	Almost Perfect	82–100%

Figure 42: Interpretation of Cohen´s Kappa (McHugh, 2012)

The confusion matrix has been processed for the four classifications with similar results between 80-85%, which indicates a strong level of agreement with a data reliability of 64%-81% following the literature (McHugh, 2012).

Confusion Matrix 1985

Class Value	C_10	C_20	C_21	C_30	C_40	C_50	C_60	C_61	C_80	kappa
U_Accuracy	0,30	0,95	0,72	0,88	0,81	1,00	0,90	0,60	0,82	
P_Accuracy	1,00	0,83	0,81	0,76	1,00	0,71	0,98	0,86	0,43	
Kappa										0,80

Table 7: Accuracy Assessment 1985

Confusion Matrix 1997

Class Value	C_10	C_20	C_21	C_30	C_40	C_50	C_60	C_61	C_80	kappa
U_Accuracy	0,90	0,93	0,58	0,80	0,92	1,00	0,91	0,90	0,92	
P_Accuracy	0,90	0,97	0,75	0,53	0,96	0,90	0,92	0,75	0,79	
Kappa										0,83

Table 8: Accuracy Assessment 1997

Confusion Matrix 2014

Class Value	C_10	C_20	C_21	C_30	C_40	C_50	C_60	C_61	C_80	kappa
U_Accuracy	1,00	0,80	0,92	0,70	0,83	1,00	0,90	0,62	1,00	
P_Accuracy	0,83	0,95	0,67	0,86	1,00	0,68	0,99	0,83	0,77	
Kappa										0,85

Table 9: Accuracy Assessment 2014

Confusion Matrix 2022

Class Value	C_10	C_20	C_21	C_30	C_40	C_50	C_60	C_61	C_80	kappa
U_Accuracy	0,28	1,00	0,46	1,00	0,92	0,75	0,87	0,46	1,00	
P_Accuracy	1,00	0,94	0,62	0,64	0,92	0,79	0,93	1,00	0,72	
Kappa										0,84

Table 10: Accuracy Assessment 2022

Comparing the four result tables there is no clear trend visible, i.e., classes that are always difficult to recognize. The results for C_20, urban cover (continuous) is in every year very high thanks to the spectral characteristics that are more easily to recognize. Likewise, the agricultural areas reach high results, both in the user´s accuracy, as in the programme´s accuracy. More difficult to recognize is the class sparsely vegetated areas, where better results are achieved in Users accuracy but weaker in the programme´s accuracy. Poor results are also received in C 21 and C 61, as they are more difficult to assign correctly due to non-uniform spectral characteristics. In cases very weak results are obtained manual corrections have to be done to receive a good performance. The k value hat to be analysed critically. If the most important categories reach high scores, the classification should be reliable and useful. The confusion matrix helps the user to understand where classified object categories have to be corrected.

3.2. Multitemporal Land Cover Change Detection

Land cover transformation in Colombia does not follow a homogeneous trend; the large Plateaus in the Andean mountains constitute areas with the highest increment of settlements (Anselm et al., 2018) and also the Bogotá Basin has historically been strongly affected by anthropogenic disturbances, mainly due to urban growth and its spreading (Romero et al., 2020). The real development of land cover change and growth of the city shall be analysed in the following

Table 11 and 12 represent a synopsis of the total development of landcover change in the selected years between 1985 and 2022. Table 11 shows the distribution in hectare per class and year, table 12 illustrates the percentage per class and year. For a thorough analysis of changes there will be taken out three examples of land cover comparison.

Category	Class	1985 in ha	1997 in ha	2014 in ha	2022 in ha
Continuous urban cover	20	1524,8	3.093,4	4.184,7	4202,1
Discontinuous urban cover	21	2785,3	1.805,1	420,0	750,6
Bare areas	30	1274,7	158,2	68,5	53,6
Forest	40	4107,9	4.303,3	4.318,0	4427,3
Shrubland	50	700,2	1.542,1	1.671,5	1956,1
Agricultural areas	60	3044,5	2.563,6	1.917,6	1833,6
Agricultural Greenhouses	61	10,2	30,2	34,1	46
Sparsely vegetated areas	80	1.594,9	1.536,0	2.411,2	1774,3

Table 11: Synopsis of class distribution in ha

Category	Class	1985 in %	1997 in %	2014 in %	2022 in %
Continuous urban cover	20	10,14	20,56	27,80	27,90
Discontinuous urban cover	21	18,51	11,99	2,79	4,98
Bare areas	30	8,47	1,05	0,45	0,35
Forest	40	27,30	28,60	28,70	29,40
Shrubland	50	4,65	10,24	11,10	12,99
Agricultural areas	60	20,23	17,03	12,70	12,19
Agricultural Greenhouses	61	0,06	0,20	0,22	0,30
Sparsely vegetated areas	80	10,60	10,20	16,00	11,79

Table 12: Synopsis of percentual distribution per class

The results of the land cover classification for the four years 1985, 1997, 2014 and 2022 can be seen in figure 43 as an overview.

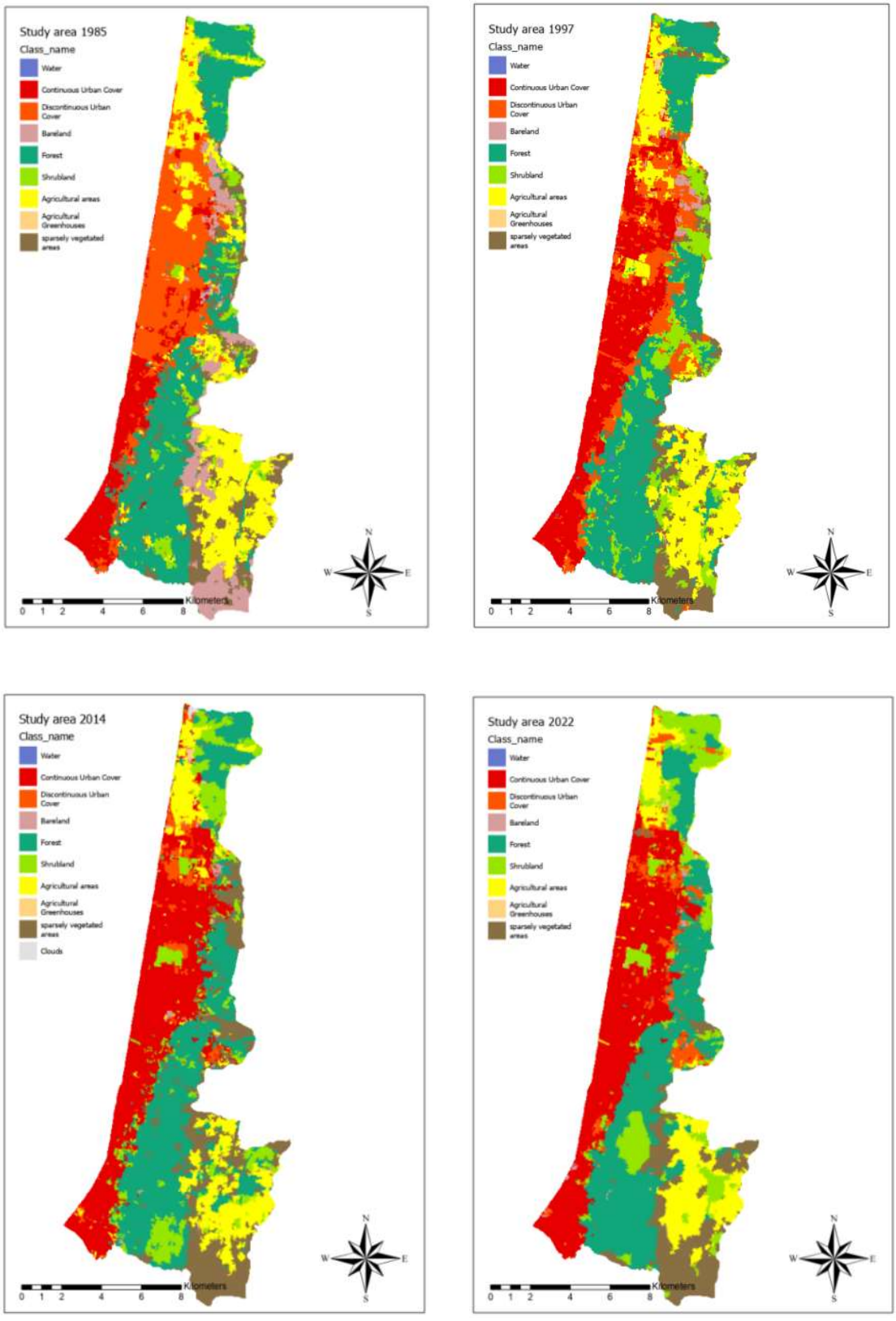

Figure 43: Land cover at 1985, 1997, 2014 and 2022

3.2.1. Comparison 1997-2014

The first comparison has been made for the years 1997 and 2014 forming the years of landslide experience. Table 13 shows the different classes in 1997 and 2014 in ha and percentage and the delta of ha to see increases or decreases per class. Important changes in categories can be noted in continuous urban cover with an increase of 35,3% and a decrease of discontinuous urban cover of 76%. This indicates a massive densification development. Bare areas represent only around 1% of land cover and do not play an important role due to its further reduction. There can be noted a considerable reduction in agricultural areas and a huge increase in sparsely vegetated areas. The share of forests remains very stable and the class shrubland increases only slightly.

Category	1997 in ha	1997 in %	2014 in ha	2014 in %	Delta ha
Continuous urban cover	3.093,4	20,56	4.184,7	27,80	35,28%
Discontinuous urban cover	1.805,1	11,99	420,0	2,79	-76,73%
Bare areas	158,2	1,05	68,5	0,45	-56,70%
Forest	4.303,3	28,60	4.318,0	28,70	0,34%
Shrubland	1.542,1	10,24	1.671,5	11,10	8,39%
Agricultural areas	2.563,6	17,03	1.917,6	12,70	-25,20%
Sparsely vegetated areas	1.536,0	10,20	2.411,2	16,00	56,98%

Table 13: Distribution of Landcover categories and their changes in 1997 and 2014

In the second table are listed the most significant changes, i.e., six aggregated shifts between one category to another in the time period 1997 to 2014 with the purpose to make the major category increases visible.

From category 1997	To category 2014	in ha	in percentage
Discontinuous Urban Cover	**Continuous Urban Cover**	1043,73	6,94
Forest	**Shrubland**	776,88	5,16
Shrubland	**Forest**	622,71	4,14
Shrubland	**sparsely vegetated areas**	561,51	3,73
Agricultural areas	**sparsely vegetated areas**	403,65	2,68
Agricultural areas	**Shrubland**	312,93	2,08

Table 14: Change in category of land cover from 1997-2014 in ha and percentage

Figure 44 and 45 visualize the areas which change their category., the white pixels mean no change in category.

From 1997 to 2014 about 60% of the land cover remains the same, the other 40% change. The highest shift between categories takes place from discontinuous urban cover to continuous urban cover. This does not come as a surprise. The change from discontinuous to continuous cover happens mainly in the north of the study area (northern Usaquén), where the relief is plane and it is easier to densify and extent the settlements. But a shift from orange to red colour can also be noted along the foot of the hills, from Usaquén in the north, to Chapinero and Santa Fe in the south (orange circles). This means that the city is extending here despite of the non-favourable topographic conditions.

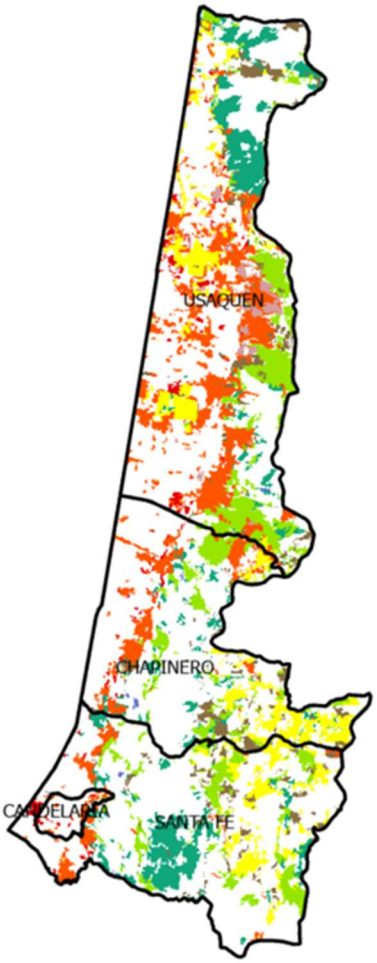

Figure 44: Land cover Change, 1997-2014, From Class (1997)

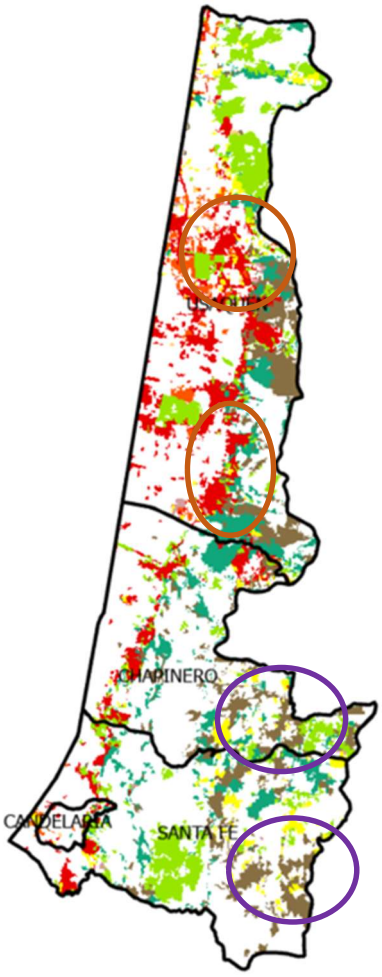

Figure 45: Land cover Change, 1997-2014, To Class (2014)

The second shift is from forest to shrubland, and vice versa from shrubland to forest. This shift can be seen in the north, in Usaquén, in the south in Santa Fe and also in the area along the border of Chapinero and Usauén. However, it seems to be a bit strange that the categories forest and shrubland change completely their colour in both directions. It seems that the spectral characteristics have not been recognized precisely in these cases. It is to assume that there is quite dense vegetational cover, but the border of these two categories is somehow vague and can therefore been seen as one whole class, namely dense vegetational cover.

Applying an approach of transition models (Rodríguez et al., 2013), the land cover dynamics can be divided in four submodels. These are the deforestation submodel, agricultural intensification, abandonment and pasture conversion submodel. For the observation time 1997 to 2014 the abandonment submodel could be of interest: a considerable decrease in agricultural cover of around 25% took place in this time period, converting it mainly in shrubland and areas with sparse vegetation. Due to migration from rural areas and the subsequent abandonment of land, the explication might be secondary vegetation on former agricultural areas.

Another reason might be a temporal one: the images have not been taken at the same time of the year: the image from 1997 is taken on August, 30th, the image 2014 is taken on January, 1st. Therefore 1997 is in winter time in the southern hemisphere, but more important, August is a month after the first annual rainy season (April/May) and counts with low precipitation amounts. Following the land cover map from 1997 the area in the eastern Santa Fe and south of Chapinero are covered with crops and green meadows, belonging to pasture and agricultural fields. The second image shows more sparsely vegetated areas in the just mentioned zone (purple circles). It is possible that at this time of the year there are more fields without crops and only little vegetation on it.

In 1997, Usaquén was covered to a higher extent with discontinuous urban cover. There are some yellow zones within coloured as agricultural areas. Here it is more about meadows as they are located in interurban area. In 2014 these areas are much smaller and now coloured in light green for shrubland. A change has taken place here owned to the process of densification; some open spaces within the city got lost.

3.2.2. Comparison 2014-2022

This comparison is intended to explain the current changes in land cover over the last 8 years. While the continuous urban cover remains stable (+0,42%), the discontinuous urban cover continues to increase by about 300ha. This occurs in the northern part of Usaquén (purple circles).

Category	Class	2014 in ha	2014 in %	2022 in ha	2022 in %	Delta ha
Continuous urban cover	20	4.184,7	27,80	4202,1	27,90	0,42%
Discontinuous urban cover	21	420,0	2,79	750,6	4,98	78,71%
Bare areas	30	68,5	0,45	53,6	0,35	-21,75%
Forest	40	4.318,0	28,70	4427,3	29,40	2,53%
Shrubland	50	1.671,5	11,10	1956,1	12,99	17,03%
Agricultural areas	60	1.917,6	12,70	1833,6	12,19	-4,38%
Sparsely vegetated areas	80	2.411,2	16,00	1774,3	11,79	-26,41%

Table 15: Distribution of Landcover categories and their changes in 2014 and 2022

Combining the two categories forest and shrubland there is also a continuous trend of increase by 400ha, while agricultural areas decrease by 100ha. Similarly, sparsely vegetated areas are reduced by 26% or almost 640ha.

The following table shows the most important movements among the categories: sparsely vegetated areas appear three times in this list as a *from category.* There are shifts toward forest, shrubland and agricultural areas. There seems to be a process of reforestation, or at least a process towards denser vegetation.

From category 2014	To category 2022	in ha	in percentage
Forest	Shrubland	873,18	5,80
Shrubland	Forest	753,21	5,00
sparsely vegetated areas	Forest	468,36	3,11
Continuous Urban Cover	Discontinuous Urban Cover	297,9	1,98
sparsely vegetated areas	Shrubland	276,75	1,84
sparsely vegetated areas	Agricultural areas	276,03	1,83

Table 16: Change in category of Landcover from 2014 to 2022 in ha and percentage

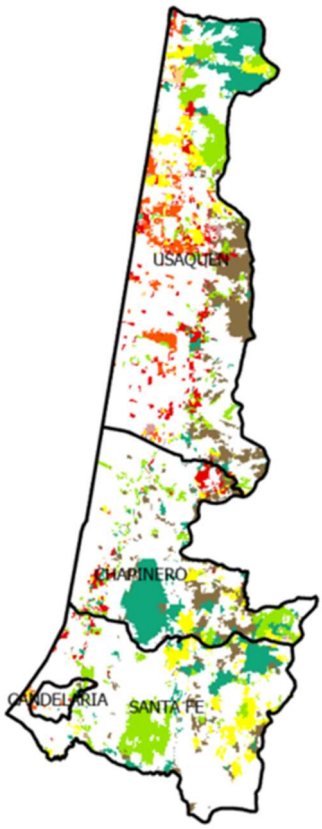

Figure 46: Land cover change, 2014-2022, From Class (2014)

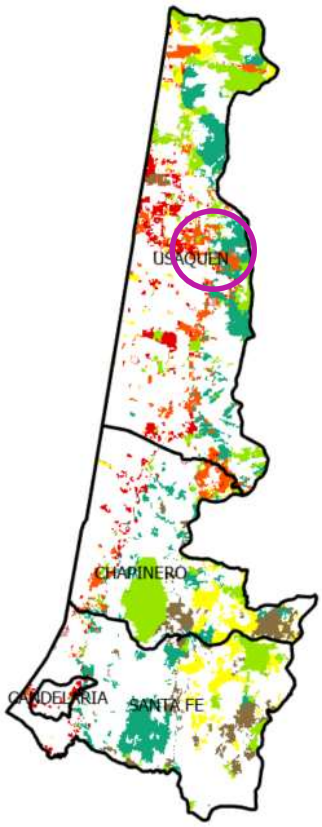

Figure 47: Land cover change, 2014-2022, To Class (2022)

As already mentioned, the number of landslides in the period 2015 to 2021 (IDIGER 3) is disproportionately high compared to the other datasets. However, at least for the study area the result of the comparison of land cover and land cover change between 2014 and 2022 does not show an increase in bare land or impending deforestation process. The reason for this significant increase in landslides must therefore be the better reporting of mass movements and the bundled data collection, at least from 2015 onwards.

3.2.3. Comparison 1985-2022

The last comparison covers the whole period from 1985 to 2022. During this time, only 45% of the total land cover remains the same. This means, that more than half of the city has changed its appearance.

Category	Class	1985 in ha	1985 in %	2022 in ha	2022 in %	Delta ha
Continuous urban cover	20	1524,8	10,14	4202,1	27,90	175,58%
Discontinuous urban cover	21	2785,3	18,51	750,6	4,98	-73,05%
Bare areas	30	1274,7	8,47	53,6	0,35	-95,80%
Forest	40	4107,9	27,30	4427,3	29,40	7,78%
Shrubland	50	700,2	4,65	1956,1	12,99	179,36%
Agricultural areas	60	3044,5	20,23	1833,6	12,19	-39,77%
Sparsely vegetated areas	80	1.594,9	10,60	1774,3	11,79	11,25%

Table 17: Distribution of Landcover categories and their changes in 1985 and 2022

When analysing this episode, the enormous shift from discontinuous to continuous urban cover becomes apparent, with more than 14% or almost 2.000 ha. The total increase in continuous urban cover is almost 2.700 ha. This can be clearly seen in the land cover change image (figure 48 and 49), namely in the change between orange and red coloured areas. In 1985, the settlements were more dispersed in Usaquén and also along the foothills. This means that the city has expanded to the north and, to a limited extent, to the east. Some new settlements can be seen in the higher areas, such as in the north of Chapinero (pink circle) and in Usaquén, which represent a further expansion of the city in the areas with high slopes.

From category 1985	To category 2022	in ha	in percentage
Discontinuous Urban Cover	Continuous Urban Cover	2171,97	14,43
Forest	Shrubland	888,39	5,90
Bareland	sparsely vegetated areas	730,71	4,86
sparsely vegetated areas	Forest	497,97	3,31
Agricultural areas	Shrubland	443,52	2,95
Shrubland	Forest	415,08	2,76
Agricultural areas	sparsely vegetated areas	343,26	2,28
Agricultural areas	Forest	323,82	2,15
Agricultural areas	Continuous Urban Cover	253,53	1,68
sparsely vegetated areas	Shrubland	239,67	1,59
Agricultural areas	Discontinuous Urban Cover	223,11	1,48

Table 18: Change in category of land cover from 1985 to 2022 in ha and percentage

Another significant change is the reduction of bare land, visible in the pink zones, which disappear completely in 2022 (purple circles). From a share up to 8,5% in 1985, bare land represents only 0,3% in 2022, a reduction of about 95%. On the one hand, bare land is transformed into sparsely vegetated areas (about 730ha), mainly in the mountains of Santa Fe and Chapinero, and on the other hand into urban cover in the north of Usaquén (about 135ha).

A further trend in the study area is a reduction of almost 40% of agricultural area in the 37 years of observation. In the north of Usaquén the reduction of agriculture is owed to the densification and extension of settlements (blue circles). In the mountainous zone of Santa Fe, where it is more about pasture, a change towards sparsely vegetated areas and shrubland is visible. The reason for a decreasing trend in agricultural use can be land abandonment due to migration from rural zones (Sánchez Cuervo et al., 2012). However, the change in land cover may also arise due to seasonal differences in land cover. Nevertheless, the table showing the most important shifts from one category to another, agricultural areas loose extent to other classes.

The area of shrubland increases almost 180% in this time. However, adding the categories shrubland and forest, taking into account the similar characteristics, the total increase is about 33%, which is still really significant.

To summarize, in 2022 the proportion of forest has increased mainly in the mountains of Usaquén (light-brown circle), and that bare areas in the mountain are being transformed into categories with at least some vegetation. In Chapinero and Santa Fe, those zones are at the highest altitudes, between 3.200 and 3.600m metres above sea level, where very little vegetation, known as *páramos*, is possible. It seems that during the last 37 years, measures have been taken to guarantee a vegetation cover, being aware of the positive effect vegetation has. This can be seen as a positive development and un

understanding of the importance of vegetation cover in reducing vulnerability to rainfall and landslides.

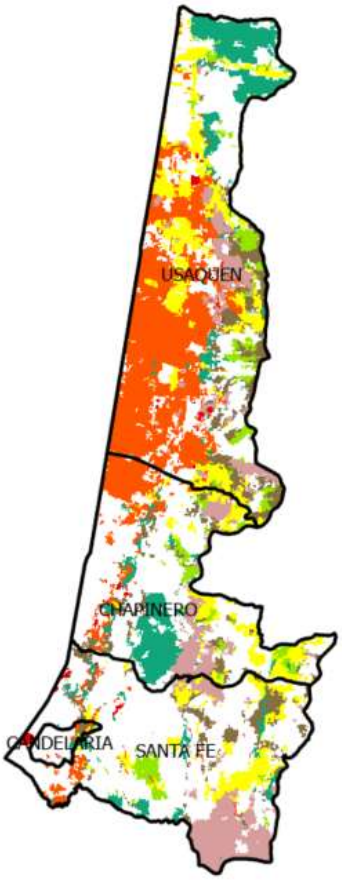

Figure 48: Land cover change, 1985-2022, From Class (1985)

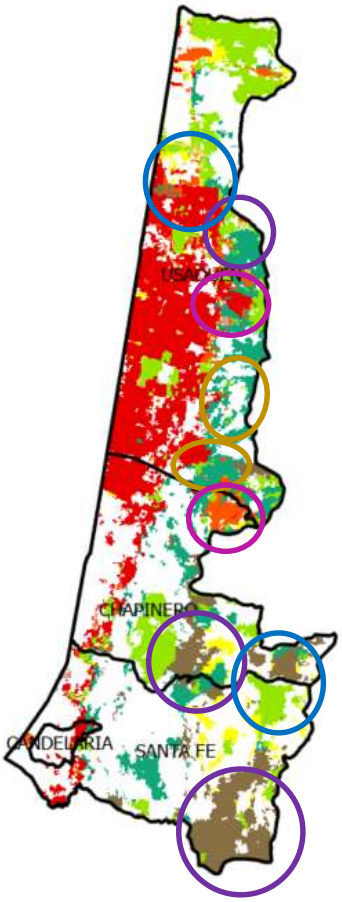

Figure 49: Landcover change, 1985-2022, To Class (2022)

3.3. Landslide assessment

For a better understanding of the cause, type and frequency of landslides, the landslide inventory was analysed and some conclusions were drawn. The following figures are based on IDIGER 5, 6 and 7, i.e., the inventory for the study area.

In order to prevent or mitigate the consequences of landslides it is important to understand the triggers. In addition to land cover and anthropogenic activities, antecedent rainfall plays an important role in Colombia in general, as it saturates the ground (Ramos et al., 2015a). With about 50% of the total number, landslides following rainfall are in first place. In second place is *damaged or lack of drainage*, which may be for the same reason, too much rainfall that cannot drain properly. The third most important factor is *human activity*. The more fragile the region, the more dangerous are human activities in that area. The massive unplanned human settlements, about 75% of the city has grown without a concept, deteriorate the stability of the hills (Yamin. L. E.; Ghesquiere, 2013). This applies not only to houses and huts, but also to roads and paths, which have been built in areas with steep slopes. Bogotá´s complex geographical and hydroclimatic environment makes the city highly vulnerable to devastating natural hazards, such as flash floods and landslides (Aristizábal and Sánchez, 2020).

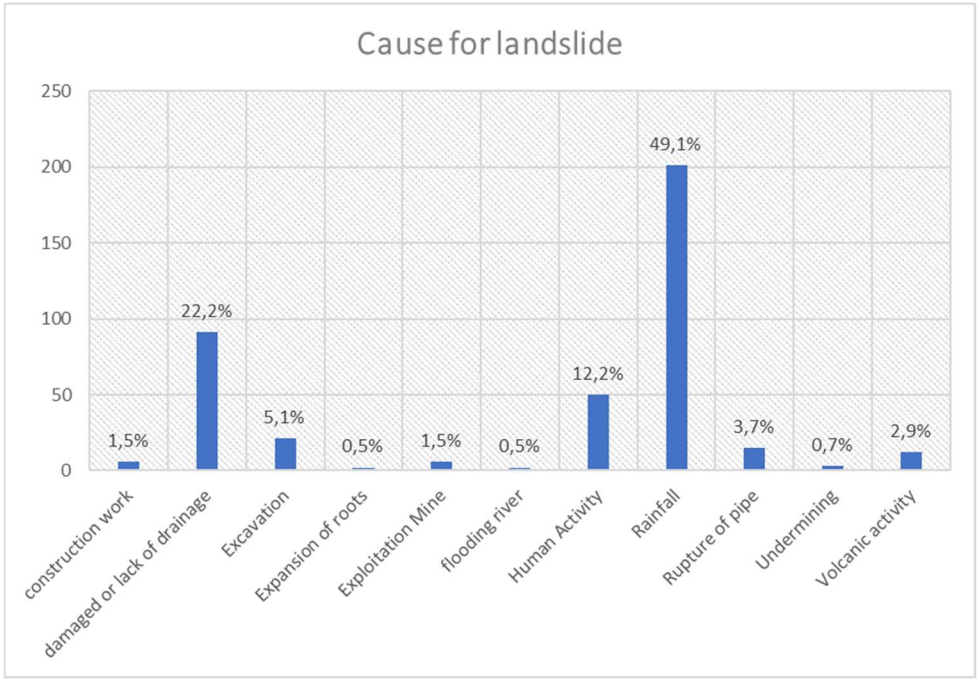

Figure 50: Cause for landslide in the Study area (IDIGER-7)

To know about the intensity of a landslide, the parameter volume of a landslide is useful. Figure 51 shows the number of landslides per year sorted according to their volume in cubic metres. The basis is IDIGER 6 with 487 landslides. Out of these landslides, about 62% take less than 5m^3 of material. Only 2% belong to the really big movements with 500-800 m^3 of material. It is obvious that the peak of total and also heavy landslides occurred between 2010 and 2012, coinciding with the La Niña period.

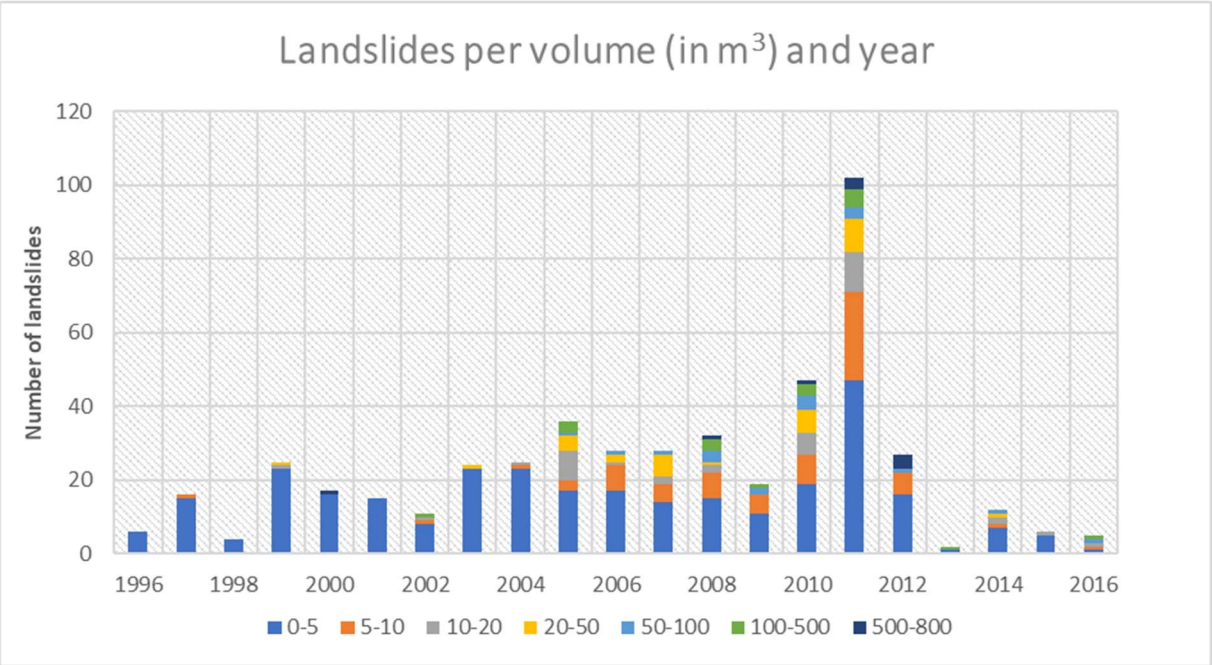

Figure 51: Number of landslides per volume and year (IDIGER 6)

Beside of the frequency in certain years there is also a relation between occurrence and time of the year: The following figure 52 shows the annual distribution of the landslides: there are two peaks, the first one in springtime, with highest values in April and May, and the second peak in November and December. The dynamic of frequency follows the two rainy seasons: the first, between March and May, lasts longer than the second, between November and December. However, the accumulated rainfall is larger in the second season (Ramos et al., 2015a). It can also be observed a lag in the landslide activity of about one or two months. Therefore, investigation purposes try to find a rainfall threshold to determine the risk of following landslides (Ramos et al., 2015a).

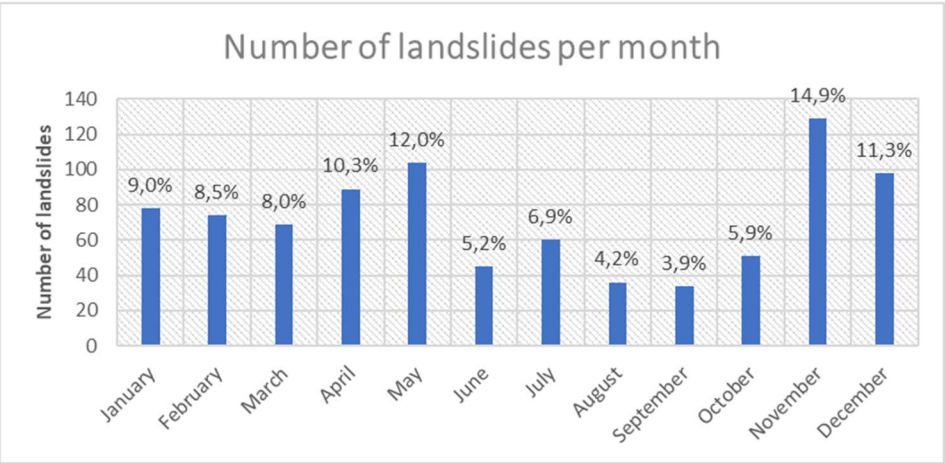

Figure 52: Landslides per month in the Study area (IDIGER-7)

The landslides are not randomly distributed in the study area. The map shows a clear clustering of landslides. There are hotspots in the south of Santa Fe and in the north of Usaquén, and generally smaller hotspots along the foothills.

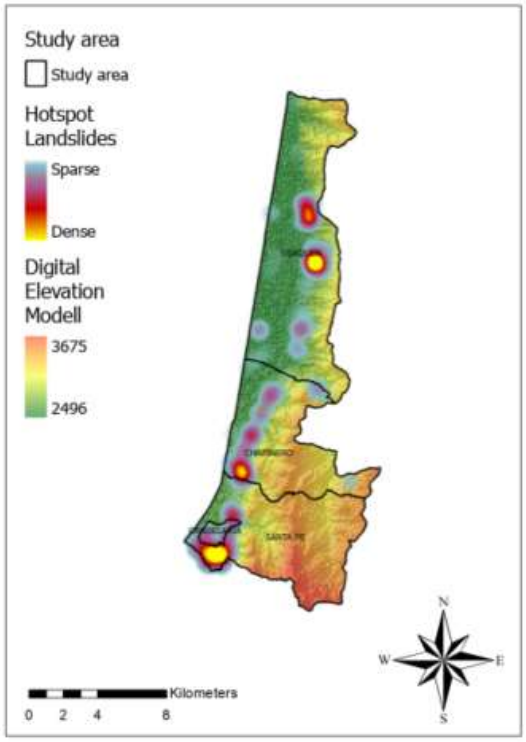

Figure 53: Landslide Hotspots in the Study area (IDIGER 5)

Comparing the hotspots with the development of settlements reveals a surprising correlation: Legalised settlements, mainly located in low socioeconomic strata, can be found precisely in these hotspots of landslide vulnerability. To sum up, vulnerability in these areas remains high due to the ever-increasing number of people living in susceptible topographic zones and the lack of minimum requirements to prevent major damages in these areas (Zamora, 2018).

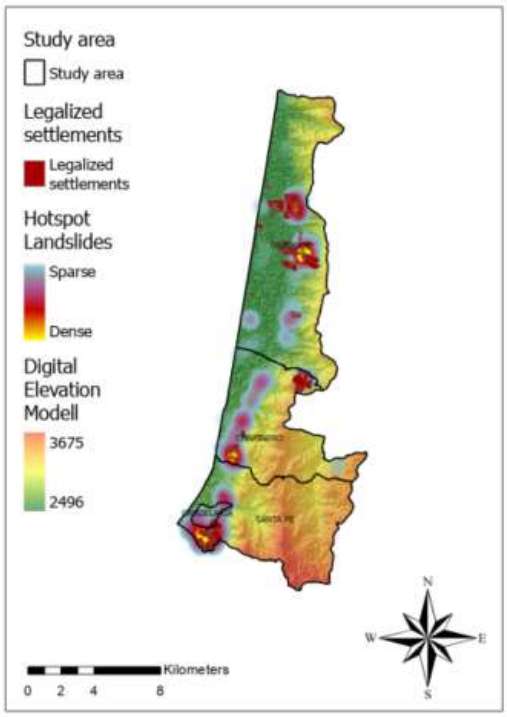

Figure 54: Legalised settlements and density of landslides (IDECA, 2022a)

3.4. Landslide Susceptibility Map

The result of the weighted categories according to their respective frequency ratio is the following map of the study area (figure 55). The Landslide Susceptibility Index ranges between 3.600 and 14.800 due to multiplication with the corresponding frequency ratio. After normalization to values between 0 and 1, the value range has been divided into five classes via Equal Breaks: very high, high, moderate, low and very low with to visualize the overall susceptibility.

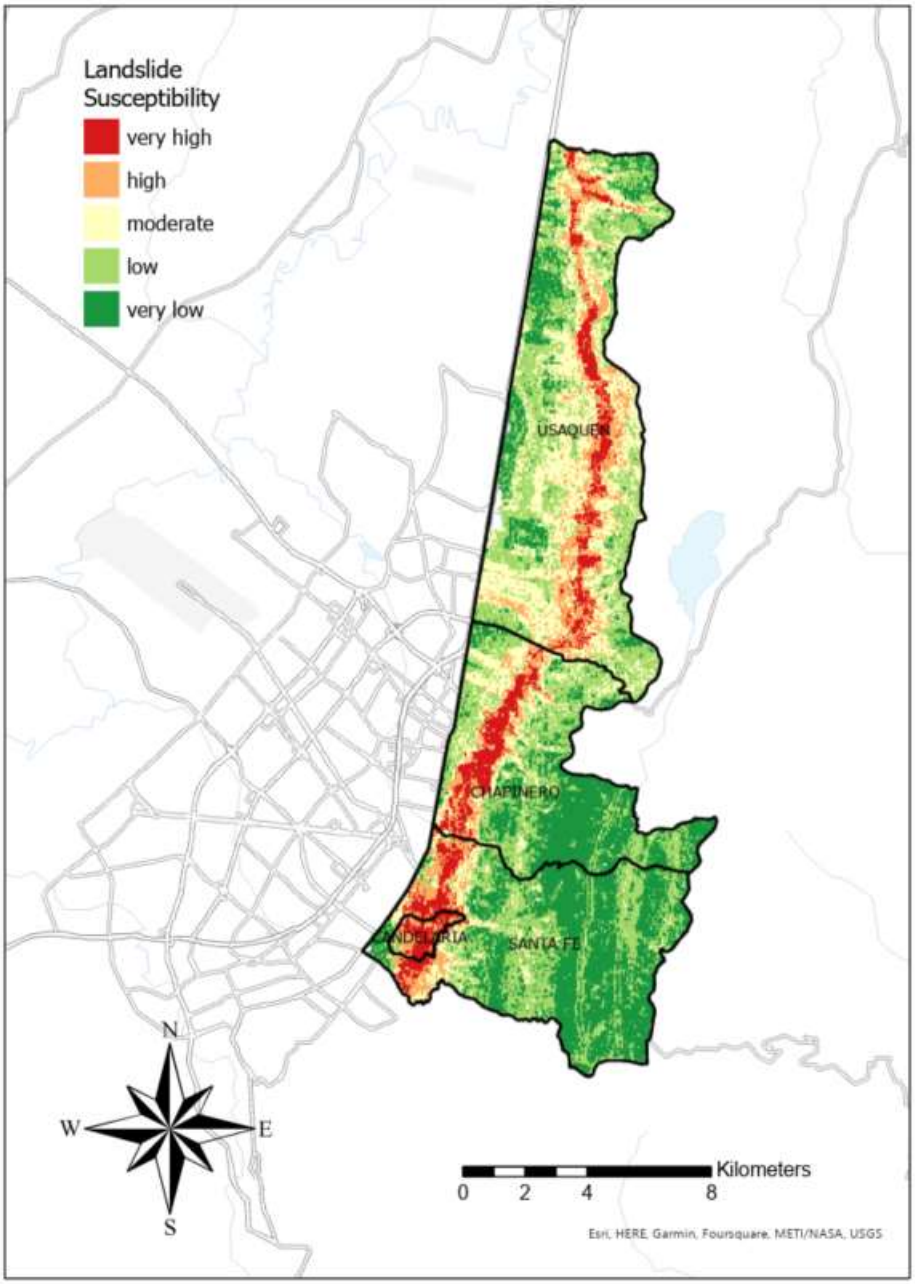

Figure 55: Landslide susceptibility map, own figure

The zones with highest susceptibility are very easily to recognize as they represent mainly the zone along the foot of the mountain range. Counting the landslides occurred in every susceptibility class, the following result as a percentage per susceptibility class can be obtained: Zone 5 with the highest LSI holds almost 47% of the total number of landslides, while in zone 4 are still 31% of all landslides.

Class	*Number*	*In percentage*
1	11	2,4
2	26	5,6
3	66	14,2
4	144	31,0
5	217	46,7

Table 19: Distribution of landslides in susceptibility map

A visual validation allows the conclusion, that the susceptibility classes reflect very well the real risk in the zones of the study area.

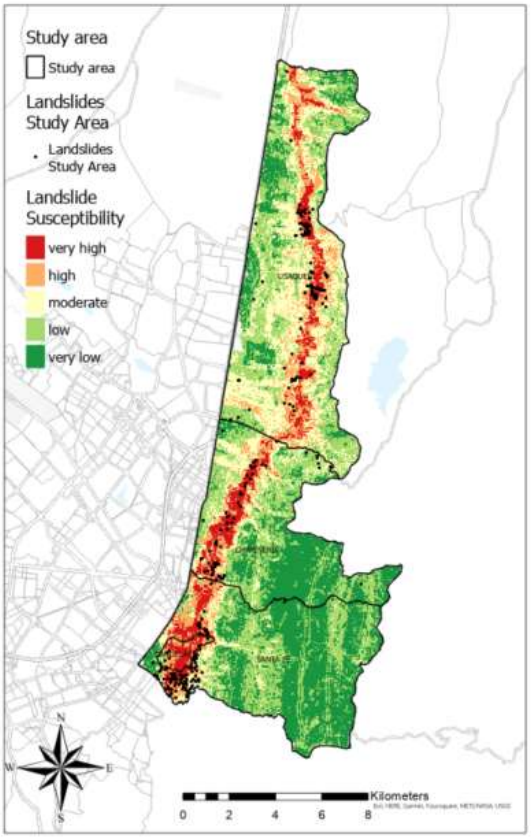

Figure 56: Landslides in Suscpetibility Map

This distribution can be interpreted in such a way, that the result of the LSM is quite reliable for the transferability of predictions of where future landslides are most likely to occur.

Taking a deeper look on the distribution of susceptibility zones, there can be drawn several conclusions out if it. According to the synopsis with all used conditioning factors and their frequency ratio, there are parameters which have a greater impact and those with less influence.

The conditioning factor with the highest frequency ratio is the distance o proximity to drainage. It can be very well seen in the below graphic, showing the northern part of Usaquén. Along the drainage system the map is coloured in red and orange, meaning a high or very high susceptibility. The smaller drainage elements show moderate susceptibility. Looking at the table with the frequency ratio for each class of this factor, there can be deducted a high correlation until a distance of 500m, with its peak at the interval of 250-500m (frequency ratio of 2,02). Smaller distances (0-200m) have a lower correlation of around 1,20.

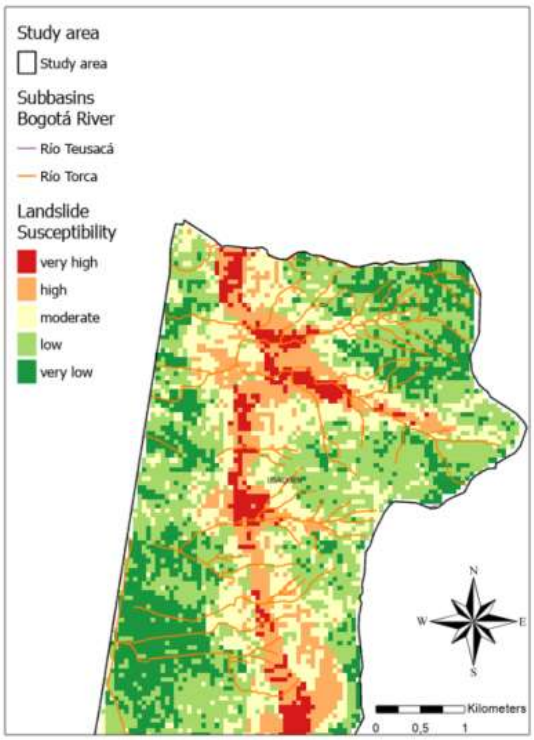

Figure 57: Impact of drainage on susceptibility

Similar to the behaviour of the distance to drainage, the Topographic Wetness Index has to be understood. The highest FR can be found in the 4th class which means high moisture values for the soil. The 5th class represents only 0,04% of the total area and there is no landslide located.

Another factor with high influence is the proximity to geological faults, with a total FR of 8,38. The map demonstrates, that along the faults the class of susceptibility is often moderate while the zones farer away belong to the class of very low susceptibility. The highest impact shows the distances between 0km and 100m from these geological faults. Distances above 500m do not correlate with landslide occurrence (FR<1).

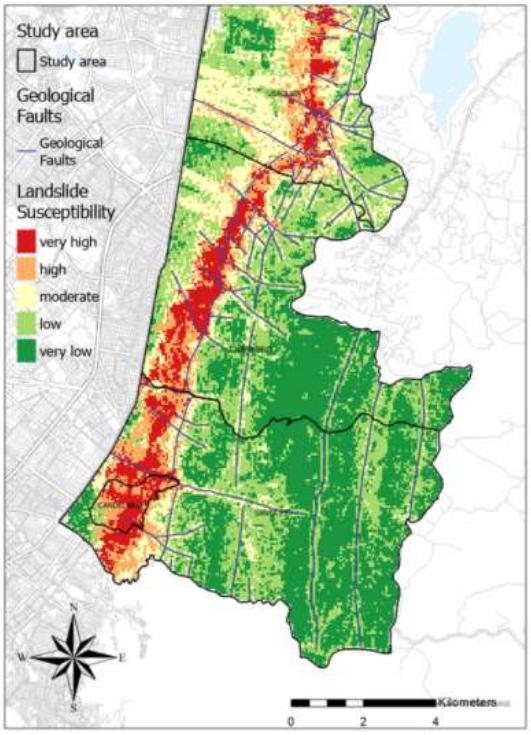

Figure 58: Impact of faults on susceptibility

A further category with high frequency ratio is the slope. However, not the steepest slopes mean the highest correlation with landslides. The highest correlation can be found in slopes of 14-24 degrees, where 33% of all landslides occur. However, looking at the absolute number of landslides, 72% of the landslides occur in slopes between 5,4° and 24, that means mainly in the areas with lower slopes. This may happen due to the weakness of point data: as only one point for the landslide is recorded, it is the point where the mass movement terminates, i.e., mainly flat zones. If also the starting point and the course of the landslide (polygon) would be considered, probably higher slopes would have higher rates of correlation.

A strict correlation can be detected between some classes of the factor aspect, namely the orientation toward the west, and in a smaller extent to the northwest and southwest. This are exactly the directions from the mountains toward the city.

Both curvature factors, plan and profile, have the lowest frequency ratio, with 4,16 and 4,91. While the results of frequency ratio in plan curvature does not have big discrepancies (between 0,34 and 1,24), in profile curvature two classes are above 1 and correlate therefore with the occurrence of landslides. Despite this correlation, these two factors help more to understand the possible way and velocity of a movement and the process of erosion and deposits due to the form of surface.

From the five geological categories, one class shows a very high correlation, i.e., the category of deposits with a frequency ratio of 3,0. To this class belong slope deposits and anthropic debris deposits, material which is not fasten to the ground moves therefore easily above all in combination with rainfalls.

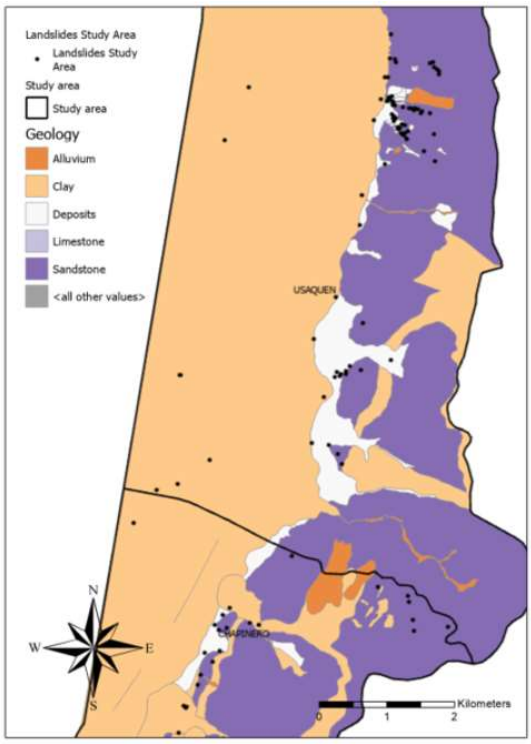

Figure 59: Deposits class with landslides

The topographic, geologic and hydrologic factors can be considered as stable, i.e., they do not change in short or midterm, while land cover is a factor that could change within a short time. Such land cover changes have a direct impact on landslide occurrence (Rahim et al., 2018). Despite the fact, that the frequency ratio for land cover is only 5,2 the distribution of the ratio within the factor has to be considered as well: While in the classes bare land (due to its small size), forest, shrubland and agricultural areas the frequency ratio is below 0,3, it is 2,86 for continuous urban cover and 1,8 for discontinuous urban cover. This indicates a strong correlation between these two classes and the appearance of landslides which can be perfectly seen in the comparison (figure 60 and 61) of susceptibility map and land cover map (purple circles). Given the fact, that the density of landslides is very low in wooded areas, the trend towards an increasing share of forest in the study area reveals a positive impact on the landslide occurrence.

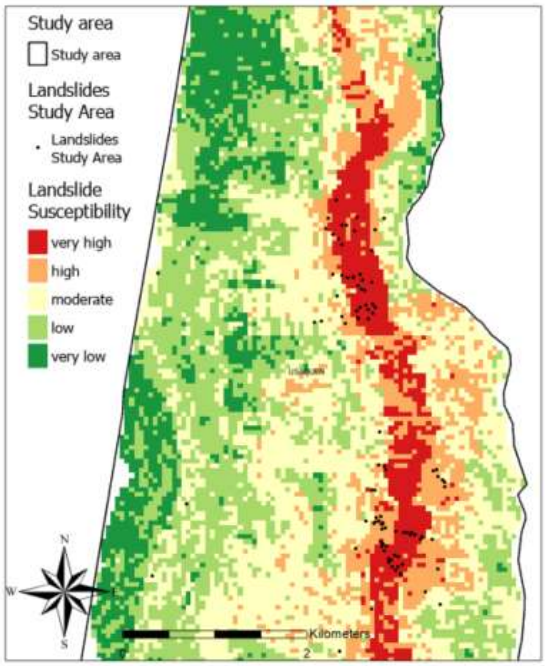

Figure 60: Part of Susceptibility Map

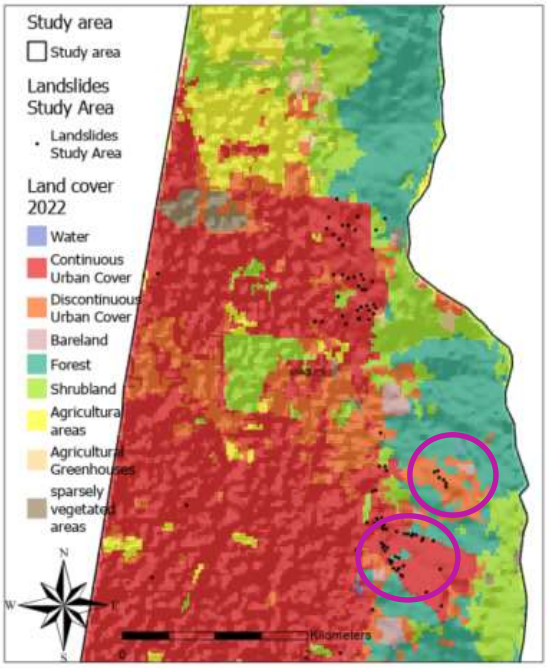

Figure 61: Part of land cover map with underlying hillshade

The following DEM map (figure 62) here divided in equal intervals, represents the same part of the map as in figure 61.

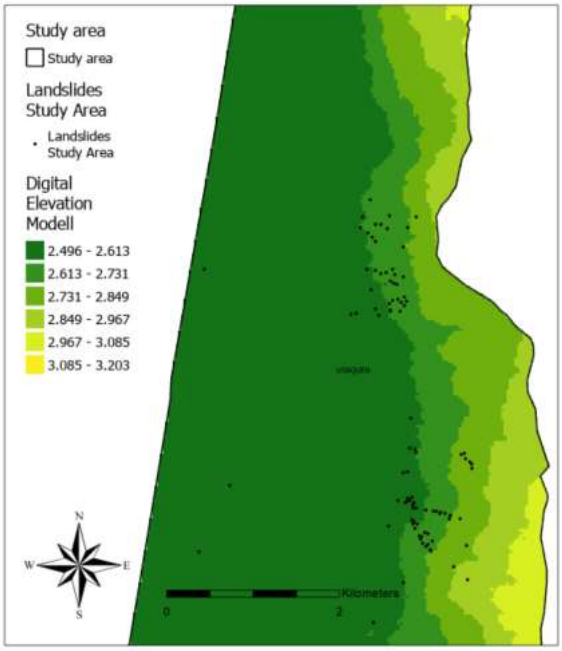

Figure 62: Part of DEM with landslides

The majority of landslides, namely about 55%, occur in an altitude of 2.613m –2.731m. This distribution of landslides signifies that the dynamic is mainly in about 100-200m above the Sabana in still populated areas. In this zone the frequency ratio is 4,51 what means an enormous correlation between this altitude and origin of landslides. The frequency ratio is also above 1 in the class 2.731-2.849m, namely

1.96 what indicates very high correlation as well. All other altitudes have a frequency ratio below 1 and therefore no influence on the formation of landslides.

In addition to the visual validation of the landslides from IDIGER 1, a second, more objective map validation is required. Therefore, a smaller landslide dataset was created based on data from SIMMA (Sistema de Información de Movimientos en Masa). This system belongs to SGC, the Colombian Geological Service, which provides landslide data for the whole country (SIMMA, 2022). Additionally, landslide data out if IDIGER-2 with a recognizable direction have been selected and merged to crosscheck if this independent inventory also matches with the created susceptibility zones.

Counting the 21 new landslides, the distribution among the classes looks like the following:

Class	*Number*	*In percentage*
1	0	0
2	1	4,7
3	3	14,3
4	7	33,3
5	10	47,6

Table 20: Distribution of validation landslides

It has to be acknowledged that the small number of landslides used for this purpose does not fulfil the requirements of a statistical validation. However, the 21 landslides are distributed very similar across the classes as the IDIGER 1 dataset. It can be therefore concluded that the LSM reflects very well the zones of highest risk.

4. Conclusion

This study has undertaken a multi-temporal assessment of land cover change. Significant changes towards a denser urban structure can be observed in the north and also in the east of the study area, but the mountain range seems to be a natural barrier that cannot be built on indefinitely. The northern part of the study area, where there are no natural barriers, experienced a much more intensive process of densification. Despite some new urban zones in the mountains, there is no trend towards deforestation of large areas in favour of new urban expansion. On the contrary, between 1985 and 2022, the area of bare land has decreased dramatically and the proportion of forest has increased by 7,8% over the same period, which, together with shrubland, represents an increase of 33% compared to 1985.

Landslides belong to the group of variable hazards that can be influenced by human activities, both negatively and positively. A long-term measure to mitigate the consequences of landslides could be reforestation, reducing the process of soil sealing and countering inappropriate practices in urban planning, effectively implementing initiatives to allow well-organised urbanisation and supporting the construction of stable houses to avoid damage from landslides and floods (BancoMundialColombia, 2012, Zamora, 2018).

The main cities in Colombia have set up several scientific institutes and governmental bodies at regional and local levels to analyse landslides, with the aim of predicting such events and protecting people and infrastructure (BancoMundialColombia, 2012). Bogotá, as the capital of the country with a high concentration of universities and institutes, is outstanding in its proactive position regarding risk management (Yamin. L. E.; Ghesquiere, 2013). Since the 1990s the city has developed several programmes to address the challenges posed by the high migratory pressure on the fragile ecosystems in which Bogotá is embedded and to reduce vulnerability to different types of natural hazards (Yamin. L. E.; Ghesquiere, 2013). The public management of Bogotá issued together with the *Secretaría de Planeación Distrital* (SDP) a so-called *Plan de Ordenamiento Territorial* (POT). This POT serves as an instrument for planning the land use of a territory taking into account the physical, social and economic aspects with strategic goals and defining the politics to achieve these goals (Zamora, 2018). The current POT for the years 2022-2035 is called *Bogotá Reverdece*, Bogotá becomes green again. While the POT of 2013 was concerned about the urban sprawl and the subsequent soil sealing, the focus is now on recognising and valuing the surrounding ecosystems and the benefit they bring to the city and the need to protect them (Bogotá/SDP, 2022).

For a successful landslide hazard management, a landslide susceptibility map can be a very helpful tool to apply an adequate planning of urban development in the exposed areas. The increasing number and the recognition of previously illegal settlements in landslide prone zones means that many more people live in exposed conditions and vulnerability increases.

In order to carry out the process of landslide susceptibility mapping, a historical dataset of landslides has been used to investigate the correlation with different conditioning factors. The landslide data were provided as point dataset. This implies a spatial limitation: only the point where the landslide

ends is recorded, not its course. Receiving the data in a polygon format also allows the origin and course of the movement to be traced, which affects a much larger area and can therefore reveal more about the correlation between the occurrence and different conditioning factors.

In addition to the influence of the ten geo-environmental factors analysed, the parameter of precipitation must also be taken into account to explain the formation of landslides. In this context the La Niña phenomenon plays an important role in explaining the frequency of landslides in a temporal sense. There is a strong correlation between the occurrence of La Niña years and the number and intensity of landslides in the study area. The knowledge of the most vulnerable zones can help to take mitigation measures, being aware of the persistence of La Niña in 2022 and the imminent risk of mass movements.

Looking to the future the question arises how landslide susceptibility will develop. On the one hand, several measures have been taken or are planned to mitigate the effects of landslides. On the other hand, in the context of climate change, the intensification of weather phenomena represents a counterweight. Future development depends mainly on the continued successful implementation of the known measures, and public awareness of the risk is essential to reduce the impact on people and infrastructure.

I. Bibliograhy

ABAD, L., HÖLBLING, D., ALBRECHT, F., DIAS, H., DABIRI, Z., REISCHENBÖCK, G. & TEŠIĆ, D. 2022. Mass movement susceptibility assessment of alpine infrastructure in the Salzkammergut area, Austria. *International Journal of Disaster Risk Reduction,* 76**,** 103009.

AKGUN, A., DAG, S. & BULUT, F. 2008. Landslide susceptibility mapping for a landslide-prone area (Findikli, NE of Turkey) by likelihood-frequency ratio and weighted linear combination models. *Environmental Geology,* 54**,** 1127-1143.

AMATYA, P., KIRSCHBAUM, D., STANLEY, T. & TANYAS, H. 2021. Landslide mapping using object-based image analysis and open source tools. *Engineering Geology,* 282**,** 106000.

ANSELM, N., BROKAMP, G. & SCHÜTT, B. 2018. Assessment of Land Cover Change in Peri-Urban High Andean Environments South of Bogotá, Colombia. *Land* [Online], 7.

ARISTIZÁBAL, E. & SÁNCHEZ, O. 2020. Spatial and temporal patterns and the socioeconomic impacts of landslides in the tropical and mountainous Colombian Andes. *Disasters,* 44**,** 596-618.

ARISTIZÁBAL, E., VÁSQUEZ, M. & RUÍZ, D. 2019. Métodos estadísticos para la evaluación de la susceptibilidad por movimientos en masa. *TecnoLógicas,* 22**,** 43-64.

BANCOMUNDIALCOLOMBIA 2012. Análisis de la gestión del riesgo de desastres en Colombia. Un aporte para la construcción de políticas públicas. *Banco Mundial Colombia and GFDRR (Global Facility for Disaster Reduction and Recovery)*.

BOGOTÁ/SDP, C. O. 2022. Bogotá reverdece con el POT. *https://bogota.gov.co/bog/pot-2022-2035/*.

CRIADO, M., SANTOS-FRANCÉS, F., MARTÍNEZ-GRAÑA, A., SÁNCHEZ, Y. & MERCHÁN, L. 2020. Multitemporal Analysis of Soil Sealing and Land Use Changes Linked to Urban Expansion of Salamanca (Spain) Using Landsat Images and Soil Carbon Management as a Mitigating Tool for Climate Change. *Remote Sensing* [Online], 12.

CRUDEN, D. 1996. Cruden,D.M., Varnes, D.J., 1996, Landslide Types and Processes, Special Report , Transportation Research Board, National Academy of Sciences, 247:36-75. *Special Report - National Research Council, Transportation Research Board,* 247**,** 76.

DATOSABIERTOSBOGOTÁ 2023. Estratificación para Bogotá. *https://datosabiertos.bogota.gov.co/dataset/estratificacion-para-bogota*.

DESINVENTAR 2020. *Sendai Framework for Disaster Risk Reduction,* https://db.desinventar.org/DesInventar/profiletab.jsp?countrycode=col&continue=y.

DIERCKEATLAS 2022. Erde-Klima. *https://webgis.diercke.de/#!/map/erde/erde-klima*.

ESRI_ARCGISPRO 2023a. Curvature function. *https://pro.arcgis.com/en/pro-app/latest/help/analysis/raster-functions/curvature-function.htm*.

ESRI_ARCGISPRO 2023b. Train Support Vector Machine Classifier (Image Analyst). *https://pro.arcgis.com/en/pro-app/latest/tool-reference/image-analyst/train-support-vector-machine-classifier.htm*.

GÓMEZ, D., GARCÍA, E. & ARISTIZÁBAL, E. 2021. *Spatial and temporal patterns of fatal landslides in Colombia*.

GÖRÜM, T. & FIDAN, S. 2021. Spatiotemporal variations of fatal landslides in Turkey. *Landslides,* 18**,** 1691-1705.

GOYES-PEÑAFIEL, P. & HERNANDEZ-ROJAS, A. 2021. Landslide susceptibility index based on the integration of logistic regression and weights of evidence: A case study in Popayan, Colombia. *Engineering Geology,* 280**,** 105958.

HOYOS, N., ESCOBAR, J., RESTREPO, J. C., ARANGO, A. M. & ORTIZ, J. C. 2013. Impact of the 2010–2011 La Niña phenomenon in Colombia, South America: The human toll of an extreme weather event. *Applied Geography,* 39**,** 16-25.

HUTCHINSON, J. N. 1988. General Report: Morphological and geotechnical parameters of landslides in relation to geology and hydrogeology. *Proceedings, Fifth International Symposium on Landslides, Rotterdam,* 1,3-35.

IDECA 2021. Corriente de Agua. Bogotá D.C. *https://www.ideca.gov.co/recursos/mapas/corriente-de-agua-bogota-dc*.

IDECA 2022a. Corriente de Agua. Bogotá D.C. *https://www.ideca.gov.co/recursos/mapas/corriente-de-agua-bogota-dc*.

IDECA 2022b. Geología Urbana. Bogotá D.C and Geología Rural. Bogotá D.C. *https://www.ideca.gov.co/recursos/mapas/geologia-urbana-bogota-dc*.

IDIGER 2018. ProcesosGeom_PG_Urbano.

KIRSCHBAUM, D., STANLEY, T. & ZHOU, Y. 2015. Spatial and temporal analysis of a global landslide catalog. *Geomorphology,* 249**,** 4-15.

KOPECKÝ, M., MACEK, M. & WILD, J. 2020. Topographic Wetness Index calculation guidelines based on measured soil moisture and plant species composition. *Science of The Total Environment*.

LEE, S. 2005. Application of logistic regression model and its validation for landslide susceptibility mapping using GIS and remote sensing data journals. *International Journal of Remote Sensing,* 26**,** 1477-1491.

LEE, S. & AB TALIB, J. 2005. Probabilistic landslide susceptibility and factor effect analysis. *Environmental Geology,* 47**,** 982-990.

LIU, Y., YUAN, A., BAI, Z. & ZHU, J. 2022. GIS-based landslide susceptibility mapping using frequency ratio and index of entropy models for She County of Anhui Province, China. *Applied Rheology,* 32**,** 22-33.

MCHUGH, M. L. 2012. Interrater reliability: the kappa statistic. *Biochem Med (Zagreb),* 22**,** 276-82.

NOAA, C. G. 2022. Climate Variability: Oceanic Niño Index. *https://www.climate.gov/news-features/understanding-climate/climate-variability-oceanic-ni%C3%B1o-index*.

POPULATIONSTAT 2022. Bogotá, Colombia Population. *https://populationstat.com/colombia/bogota*.

POVEDA, G., JARAMILLO, A., GIL, M., QUICENO, N. & MANTILLA, R. 2001. Seasonality in ENSO related precipitation, river discharges, soil moisture, and vegetation index (NDVI) in Colombia. *Water Resources Research,* 37**,** 2169.

RAHIM, I., ALI, S. M. & ASLAM, M. 2018. GIS Based Landslide Susceptibility Mapping with Application of Analytical Hierarchy Process in District Ghizer, Gilgit Baltistan Pakistan. *Journal of Geoscience and Environment Protection,* 06**,** 34-49.

RAMESH, V. & ANBAZHAGAN, S. 2014. Landslide susceptibility mapping along Kolli hills Ghat road section (India) using frequency ratio, relative effect and fuzzy logic models. *Environmental earth sciences,* 73**,** 8021.

RAMOS, A., PRADA SARMIENTO, L., TRUJILLO-VELA, M., MACÍAS, P. & SANTOS, A. 2015a. Linear discriminant analysis to describe the relationship between rainfall and landslides in Bogotá, Colombia. *Landslides*.

RAMOS, A., TRUJILLO-VELA, M. & PRADA SARMIENTO, L. 2015b. Análisis descriptivos de procesos de remoción en masa en Bogotá. *Obras y proyectos***,** 63-75.

RODRÍGUEZ, N., ARMENTERAS, D. & ALUMBREROS, J. 2013. Land use and land cover change in the Colombian Andes: Dynamics and future scenarios. *Journal of Land Use Science,* 8**,** 154-174.

ROMERO, C. P., GARCÍA-ARIAS, A., DONDEYNAZ, C. & FRANCÉS, F. 2020. Assessing Anthropogenic Dynamics in Megacities from the Characterization of Land Use/Land Cover Changes: The Bogotá Study Case. *Sustainability* [Online], 12.

SÁNCHEZ CUERVO, A. M., NCHEZ-CUERVO, S., AIDE, T. M., CLARK, M. & ETTER, A. 2012. Land Cover Change in Colombia: Surprising Forest Recovery Trends between 2001 and 2010. *PLoS ONE,* 7**,** 1-14.

SARMIENTO, J. P., HOBERMAN, G., ILCHEVA, M., ASGARY, A., MAJANO, A. M., POGGIONE, S. & DURAN, L. R. 2015. Private sector and disaster risk reduction: The Cases of Bogota, Miami, Kingston, San Jose, Santiago, and Vancouver. *International Journal of Disaster Risk Reduction,* 14**,** 225-237.

SDP 2022. Visor de Población Bogotá D.C. *https://sdpbogota.maps.arcgis.com/apps/MapSeries/index.html?appid=2ac7960e89eb44709bc2dcae1eb96fb9*.

SGC, S. G. C. 2022. Mapa Nacional de Amenaza por Movimientos en Masa. http://geoportal.sgc.gov.co/Flexviewer/Amenaza_Movimiento_Remocion_Masa/.

SIMMA 2022. Catálogo de movimientos en masa. *Sistema de Información de Movimientos en Masa, Servicio Geologico Colombiano*.

SOLAIMANI, K., MOUSAVI, S. & KAVIAN, A. 2012. Landslide susceptibility mapping based on frequency ratio and logistic regression models. *Arabian Journal of Geosciences,* 6.

TEŠIĆ, D., ĐORĐEVIĆ, J., HÖLBLING, D., DJORDJEVIC, T., BLAGOJEVIĆ, D., TOMIC, N. & LUKIĆ, A. 2020. Landslide Susceptibility Mapping Using AHP and GIS Weighted Overlay Method: A Case Study from Ljig, Serbia. 6**,** 9-21.

USGS, U. S. D. O. T. I. 2007. Scenario generation for long-term water budget analysis using the TOPMODEL rainfall-runoff model. *Alambama Water Resources Conference*.

USGS_EARTH_EXPLORER 2013. ASTGTMV003_N04W074.zip and ASTGTMV003_N04W075.zip. *https://earthexplorer.usgs.gov/,* 10.5067/ASTER/ASTGTM.003.

WORLDBANK 2021. Köppen-Geiger Climate Classification, 1991-2020. *https://climateknowledgeportal.worldbank.org/country/colombia*.

WORLDBANK 2022. Colombia receives US$300 million World Bank disbursement to support itr response to La Nina.

YAMIN. L. E.; GHESQUIERE, F. C., O. D.; ORDAZ, M. G 2013. Modelación probabilista para la gestión del riesgo de desastre. El caso de Bogotá, Colombia. *Banco Mundial, Universidad de los Andes Colombia*.

ZAMORA, N. 2018. THE LANDSLIDE HAZARD MAP OF BOGOTA AN UPDATING. *ISPRS - International Archives of the Photogrammetry, Remote Sensing and Spatial Information Sciences,* XLII-4/W8**,** 233-241.

II. Science Pledge

I hereby declare that this master thesis is entirely the result of my work. I have cited all sources I have used din my thesis and always indicated their origin. This thesis was not previously presented to another examination board and has not been published.

Ravensburg, March 5th, 2023